Geospatial micro-estimates of slum populations in 129 Global South countries using machine learning and public data

Dan Li[a], Laixiang Sun[b,c,*], Yang Yu[d], Peipei Tian[a]

[a] Institute of Blue and Green Development, Shandong University, Weihai, 264209, China

[b] Department of Geographical Sciences, University of Maryland, College Park, 20742, MD, USA

[c] School of Finance & Management, SOAS University of London, London, WC1H 0XG, UK

[d] Division of Liberal Studies, Howard Community College, Columbia, MD 21044, United States.

* Corresponding author: lsun123@umd.edu (L.S.)

Abstract

Slums are a visible manifestation of poverty in Global South countries. Reliable estimation of slum population is crucial for urban planning, humanitarian aid provision, and improving well-being. However, large-scale and fine-grained mapping is still lacking due to inconsistent methodologies and definitions across countries. Existing datasets often rely on government statistics, lacking spatial continuity or underestimating slum population due to factors such as city image and privacy concerns. Here, we develop a standardized bottom-up approach to estimate the slum population at the grid-cell ~~neighborhood~~ level (~6.72 km resolution at the equator) for 129 Global South countries in 2018. Leveraging the Sustainable Development Goals 11.1 framework and machine learning, our estimation integrates household-based surveys, satellite imagery, and grided population data. Our models explain 82% to 96% of the variation in ground-truth surveys, with a root mean squared error of 4.85% to 10.47%, outperforming previous benchmarks. Cross-validation with independent data confirms the reliability of our estimates. To our knowledge, this is the first comprehensive geospatial inventory of slum populations across Global South countries, offering valuable insights for advancing urban sustainability and supporting further research on vulnerable populations. The maps of slum populations and their local shares in Global South countries are available in the Zalando repository at https://doi.org/10.5281/zenodo.13779003 (Li et al., 2025).

Introduction

The right to adequate housing and shelter holds a central position in the realm of international human rights (Hohmann, 2013; Nowak, 2021). However, a distressing reality persists: millions of individuals worldwide live in life- or health-threatening conditions, commonly referred to as slums, informal settlements, favelas, or shanties (Hardoy et al., 2013). As a kind of visible expressions of poverty, slums are typically characterized by physical state of disrepair, degraded environment in insanitary conditions, and absence of basic and essential facilities, and they are often situated in disadvantageous, exposed and hazardous areas (Abascal et al., 2022; UN-Habitat, 2004). The emergence and persistence of slums have been a consequence of rapid and unplanned urbanization that outpaces economic growth and infrastructure development (Ezeh et al., 2017; Marx et al., 2013). According to the World Cities Report 2020 (UN-HABITAT, 2020), over 1 billion people live in urban slums, with 80% of them residing in cities within developing countries. Nevertheless, urbanization has not yet peaked, and the population living in slum-like conditions is expected to grow (Guan et al., 2018; UN-HABITAT, 2020). This intensifies the urgency to provide adequate housing, basic services and slums upgrades, in line with the commitment to the Sustainable development Goals (SDG) and “leaving no one behind” (Weber, 2018; Tian et al., 2024).

Reliable slum population estimates are essential for understanding the spatial scale and distribution of slum populations, providing foundational data for implementing targeted urban planning and improving human well-being (Parikh et al., 2013; Satterthwaite et al., 2020; Schetke et al., 2012). These estimates help identify vulnerable populations, similar to demographic data on the elderly and women (Singh, 2016). Detailed knowledge of slum population locations enables effective resources allocation and targeted interventions (Doe et al., 2020; Zhou et al., 2022). Quantitative data can also motivate policymakers and researchers to tackle inequalities, while spatial knowledge can help pinpoint drivers of slum population growth, such as proximity to rivers and elevation, thus contributing to climate risk management (Baynes et al., 2022; Rentschler et al., 2023; Sietchiping and Yoon, 2010).

Despite this, large-scale, comparable inventories of slum populations remain scarce. National statistics and sparce survey data, such as those from censuses or Know Your City Campaigns, fail to provide a spatially continuous view of slum population (Angeles et al., 2009; Pedro and Queiroz, 2019; Persello and Kuffer, 2020). These data collections are inconsistent across countries (Thomson et al., 2020), and governments may withhold or omit sensitive information due to factors such as city image considerations (Björkman, 2013; Moreno, 2003; Wurm et al., 2017). Privacy concerns also contribute to underreporting (Engin et al., 2020), as slum dwellers may distrust external inquiries (Binzel and Fehr, 2013; Rogler, 1967). As a result, spatially explicit data on slum populations, particularly in developing countries, remain scarce.

Recent advancements in machine learning and the availability of satellite imagery provide new opportunities for slum population mapping (Burke et al., 2021; Gram-Hansen et al., 2019; Wurm et al., 2019). While considerable research has focused on identifying slums based on satellite-derived morphological features, such as studies in Mumbai (Ibrahim et al., 2019), and Kenya (Mahabir et al., 2020), these efforts are often limited to individual cities (Banerjee et al., 2017;

Thomson et al., 2020) and may not provide comparable results across countries or regions. For instance, the boundaries of slum determined in these studies may yield discrete outcomes (Patel et al., 2019), making it difficult to integrate this information with population data to produce large-scale demographic insights (Breuer and Friesen, 2023). In some cases, there might be a necessity to obfuscate the precise boundaries of slums to safeguard the privacy of already vulnerable populations (Thomson et al., 2019). Although several studies have estimated slum populations in selected cities across the Global South, these estimates are generally considered to be underestimations (Breuer et al., 2024; Thomson et al., 2022).

In this study, we integrate ground-surveys, public satellite imagery, and advanced machine learning to map slum population at the grid~~cluster~~-cell level (6.72km × 6.72km at the equator) across Global South countries. During the training, validation, and testing phases, we assemble data from surveys covering over 1 million households in 67,204 clusters across 53 countries, sourced from Demographic and Health Surveys (DHS). Using this data, we construct a slum indicator framework and fine-tune the ResNet-34 algorithm to extract features from Landsat and nighttime light imagery. For out-of-sample predictions, we apply the cross-validated model to predict slum indicators and integrate them with grided population data to create detailed slum population maps for 129 Global South countries in 2018. The 129 countries in the Global South are identified according to the list provided by the United Nations Conference on Trade and Development (UNCTAD, 2025). Overall, we offer a generalized and scalable approach to slum population mapping that enables regional comparisons while maintaining privacy safeguards. The objectives of this study are to (1) develop a machine learning-based workflow for slum population mapping, (2) generate a fine-grained inventory of slum population in 129 Global South countries, and (3) analyze spatial distribution disparities across different geographic regions and income groups.

2 Dataset description

Four types of publicly accessible datasets are used in this study. The first type is geo-referenced household surveys, which are used to calculate the slum indicator as machine learning labels. The second type consists of daytime satellite imagery and nighttime light imagery, which serve as the input features. The third type is grided population data, used in combination with the slum indicator to produce the final gridded slum population estimates. The fourth type consists of gridded auxiliary data related to slum populations, which help exclude areas without human settlements. Table 1 outlines the datasets and layers that are used to generate the slum population map in this study.

Table 1. Overview of data sources for generating the slum population map in Global South countries

Data Sources	Abbreviation	Input spatial resolution	Period Coverage	Reference
Demographic and Health Survey	DHS (https://www.dhsprogram.com/Data/)	household-based data, ~2km for urban areas and ~5km sometimes 10km for rural areas	The latest version for 53 countries varying from 2010~2020	Rutstein and Staveteig (2014)
Landsat Collection 2 on Google Earth Engine	Landsat 8 Level 2, Collection 2, Tier 1 (https://developers.google.com/earth-engine/datasets/catalog/LANDSAT_LC08_C02_T1_L2) Landsat 7 Level 2, Collection 2, Tier 1 (https://developers.google.com/earth-engine/datasets/catalog/LANDSAT_LE07_C02_T1_L2)	30m	Landsat 7 ETM+: 1999~2024 Landsat 8 OLI/TIRS: 2013~2024	Taminimia et al. (2020); Roy et al. (2016)
Global NPP-VIIRS-like nighttime light data (through a new cross-sensor calibration from DMSP-OLS NTL data and a composition of monthly NPP-VIIRS NTL data.	An extended time-series (2000-2023) of global NPP-VIIRS-like nighttime light data (https://doi.org/10.7910/DVN/YGIVCD)	15 arcsec (~500 m)	2000~2023	Chen et al. (2021~~0~~); Elvidge et al. (2017); Hsu et al. (2015)
Global Human Settlement Population Grid	GHS-POP (https://human-settlement.emergency.copernicus.eu/download.php?ds=pop)	1km	2020	Schiavina et al. (2022)
Global Human Settlement Model Grid	GHS-SMOD (https://human-settlement.emergency.copernicus.eu/download.php?ds=smod)	1km	2020	Schiavina et al. (2022)
Copernicus	Copernicus Global Land Cover Layers: CGLS-LC100 Collection 3 (https://developers.google.com/earth-engine/datasets/catalog/COPERNICUS_Landcover_100m_Proba-V-C3_Global)	100m	2018	Buchhorn et al. (2020)

2.1 Geo-referenced household surveys

This study uses the household-based ground survey data from Demographic and Health Surveys (DHS) to calculate the proportion of slum households for each ~~at the~~ cluster~~r-level~~. Here, a cluster refers to a DHS enumeration unit, approximately the size of a neighbourhood or village. The DHS program is funded primarily by the United States Agency for International Development (USAID), and collects nationally representative and comparable information based on a consistent set of questionnaires for a wide range of monitoring and impact evaluation indicators in the areas of population, health, and household living conditions in developing countries (Rutstein and Staveteig, 2014). The derived standard DHS Surveys have large sample sizes (usually between 5,000 and 30,000 households) and typically are conducted about every 5 years. Focusing on Global South countries, we de~~p~~rive the geo-referenced data from 53 countries (as of 2022) in Latin American, Africa and Asia, with a valid dataset comprising over 1 million households across 67,204 clusters. The ground-truth household surveys points can be found in Figure S1 and Table S1. To protect respondent confidentiality, the DHS program randomly displaces the geographic coordinates of the surveyed locations, with a maximum of 2km for urban clusters and 5km or sometimes 10 km for rural clusters (Burgert et al., 2013). To avoid misclassification in analysis using administrative-level data, the displacements are constrained within the administrative boundaries, specifically at the administrative level 3 (Figure S2). The cluster ~~level~~ thus corresponds to neighborhoods in urban areas or villages in rural areas.

2.2 Satellite imagery

We obtained publicly available Landsat-7 ETM+~~collect publicly available Landsat-7 ETM+~~ (Collection 2, Tier 1), Landsat-8 OLI (Collection 2, Tier 1) and nighttime light imagery ~~centered on each cluster~~ from Google Earth Engine platform (Taminimia et al., 2020) , along with the Global NPP-VIIRS-like nighttime light dataset~~and Global NPP-VIIRS-like nighttime light dataset~~ (Chen et al., ~~2020~~2021). The Landsat imagery series provides the world's longest-running collection of consistently acquired, high-resolution Earth observation data and have been widely applied in studies such as urban growth monitoring ~~Landsat imagery series offer the world's longest-running collection of consistently acquired, high-resolution earth observation data, and have been applied in numerous studies such as urban growth monitoring~~ (Patel et al., 2015; Wulder et al., 2022). The collection 2, Tier 1 images have undergone improved systematic geometric correction and radiometric calibration. Due to differences in the spectral reflectance between different sensors, we adopt the normalization coefficients from Roy et al. (2016) to characterize the ETM+ reflectance to that of OLI. To get clear slices with fewer clouds and snow, we generate a 1-year median composite from Landsat imagery by selecting cloud-free pixels based on the quality assessment (QA) bands, and then calculating the median value for each available cloud-free pixel over the 1-year period (Azzari and Lobell, 2017). Similarly, considering the inconsistent timing of household surveys across countries, we use the Global NPP-VIIRS-like nighttime light dataset to ensure spatiotemporal consistency between satellite imagery and slum indicator labels. This NPP-VIIRS-like dataset is particularly suitable for analyzing long-term demographic and socioeconomic trends, as its cross sensor calibration between DMSP OLS (2000 – 2012) and NPP VIIRS (2013 – 2018) removes inter sensor bias and drift, yielding a radiometrically consistent time series~~This NPP-VIIRS-like dataset, produced through cross-sensor calibration of the DMSP-OLS and NPP-VIIRS datasets, is particularly suitable for analyzing long-term demographic and socioeconomic trends.~~ (Chen et al., 2021). We thus obtain six multispectral bands from Landsat imagery including red, green, blue, near infrared and two shortwave infrared bands, and one single band from NPP-VIIRS-like nighttime light dataset. The input images used for model training are centered on the geographic coordinates of each DHS cluster, using a standardized grid cell size of approximately 6.72 km to ensure spatial alignment with the corresponding DHS labels. For map generation, images are collected for every 6.72 km grid cell across the study area, enabling the production of spatially continuous predictions. The Landsat and Nighttime light slices have a size of 224 × 224 tiles, in accordance with the input size of our convolutional neural networks architecture and covering the extent of displacement. Consequently, our mapping resolution is determined to be 6.72 kilometers ~~on~~ at the equator (30m-pixel size × 224 pixels = 6.72 km).

2.3 Population and gridded auxiliary data

We utilize and process the 1km-gridded Global Human Settlement Population dataset (GHS-POP), developed by the EU Joint Research Center, to estimate the slum population (Schiavina et al., 2022). The GHS-POP dataset provides a more precise estimation of population distribution by disaggregating census or administrative unites into grid cells, based on the classification of built-up areas in the Global Human Settlement Layer derived from Landsat imagery. It is selected for its superior accuracy and top-down constrained allocation approach, outperforming other available gridded population datasets (Smith et al., 2019; Tellman et al., 2021). We resample this population dataset to match the resolution of our grid-cell~~cluster~~ level mapping. Additionally, we incorporate the GHS Settlement Model Grid (GHS-SMOD) and the Copernicus Global Land Cover Layers product (CGLS-LC100) as auxiliary grided data (Buchhorn et al., 2020; Schiavina et al., 2022). This helps us differentiate settlement patterns across urban, semi-urban, and rural areas, and also allows us to exclude areas with low population density.

3 Methodology

We propose a standardized and comparable framework for estimating ~~cluster~~grid-cell level slum population, which integrates a slum indicator framework based on the definition of slum households, a deep learning model, and an XGBoost ensemble classifier. Our approach addresses the underestimation of slum population in prior literature, which heavily relied on slum boundary geometry. A set of examples of the uncertainties in slum boundary delineation is shown in Figure S3. Figure 1 depicts the flowchart for mapping slum populations in Global South countries. The main procedures are outlined as follows.

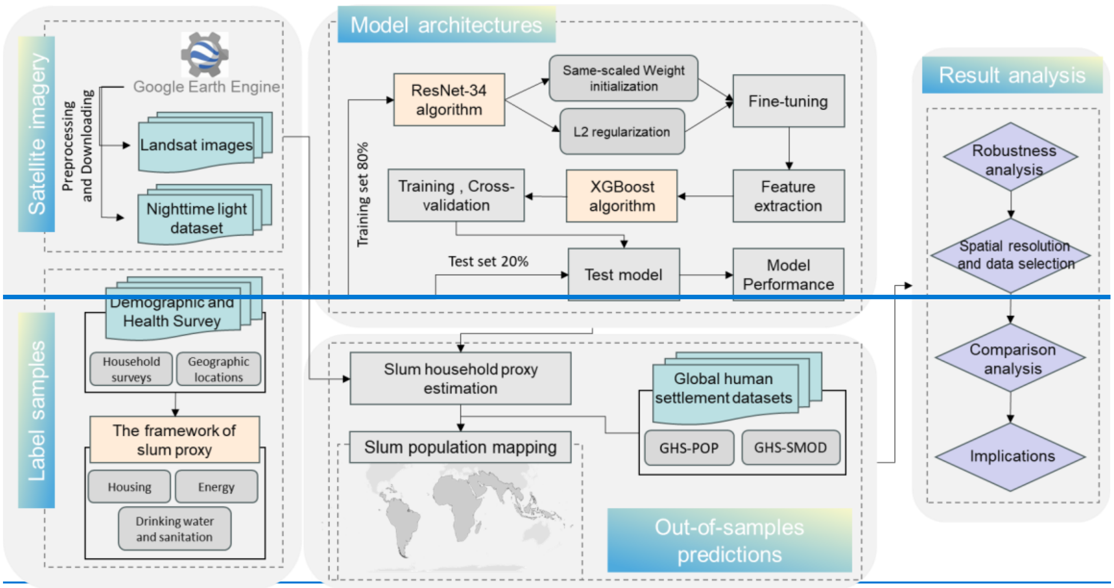

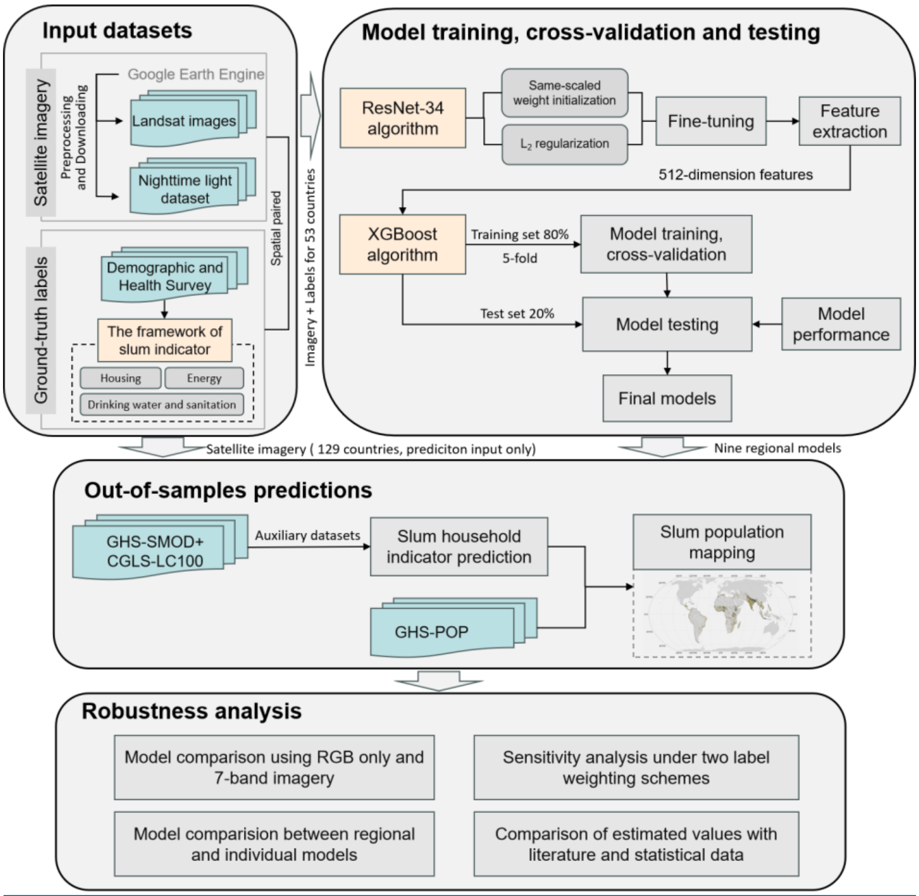

Figure 1 Workflow of this study. Blue backgrounds represent datasets, yellow backgrounds indicate the indicator framework or model architecture, and gray backgrounds denote specific processes or procedural steps.~~Figure 1 Flowchart of this study~~

3.1 Framework of slum indicator

We use the SDG 11.1 framework as a proxy to estimate the occurrence of households living in slums or slum-like conditions within a cluster. Based on UN-Habitat's definition of a slum household (UN-habitat, 2021), we incorporate "access to electricity" into our slum population framework, recognizing its critical role in human well-beings in developing countries. However, we exclude the "security of tenure" dimension due to data limitations. As a result, the slum population is defined as individuals (or households) living in conditions lacking one or more of the following: safely and adequate housing, safely managed drinking water and sanitation services, or reliable and modern energy services. These conditions are categorized into three dimensions, comprising ten indicators (Table 2). The specific definitions and criteria are detailed in Table S2. We treat housing, water and sanitation, and electricity as equally important, assigning each a weight of 0.33. The slum indicator is then determined as follows:

$$S_c = \frac{1}{NH_c} \cdot \left(w_H \cdot \frac{\sum_{i=1}^{n_H} h_{i,c}}{n_H} + w_W \cdot \frac{\sum_{j=1}^{n_W} wa_{j,c}}{n_W} + w_E \cdot \frac{\sum_{l=1}^{n_E} e_{l,c}}{n_E}\right) \cdot 100\% \qquad (1)$$

where S_c represents the slum indicator for each cluster c; NH_c is the total number of households in cluster c; w_H, w_W, and w_E represent the weights assigned to the dimensions of safely and adequate housing (H), safely managed drinking water and sanitation services (W), and reliable and modern energy services (E); n_H, n_W, n_E represent the total number of sub-indicators within the H, W and E dimensions, respectively; $h_{i,c}$, $wa_{j,c}$, and $e_{l,c}$ denote the numbers of households in cluster c that fail to meet the criteria for the i-th housing sub-indicator, j-th water and sanitation sub-indicator, and l-th energy sub-indicator, respectively.

The DHS surveys' standardized instruments and rigorous quality control protocols ensure high reliability of the data, which in turn supports the validity of our labels. Before constructing the slum household indicator, we applied a comprehensive data cleaning process. Sub-indicator with missing values, "don't know" responses, or implausible entries were excluded. If all sub-indicators within a given dimension were missing, the corresponding household record was removed. Clusters with invalid GPS coordinates were also excluded. Additionally, to evaluate the sensitivity of the labels to the indicator weighting scheme, we implemented two alternative weighting scenarios (see Section 3.5 for more details).

Table 2 The framework of slum indicator based on household data

Dimensions	Indicators
Safely and adequate housing	House made of finished materials (roof, wall and floor)
	House with a sufficient living room
Safely managed drinking water and sanitation services	Household using safely managed drinking water
	Household with access to water availability for continuous two weeks
	Household with access to drinking water located within a round trip of 30 minutes
	Household using safely managed sanitation toilets
	Household using safely managed hand-washing facility with water.
	Household using safely managed hand-washing facility with soap or detergent
Reliable and modern energy services	Household with access to electricity
	Household with clean cooking fuels

3.2 Model architecture

We employ transfer learning by fine-tuning the pre-trained ResNet-34 to extract the informative features from satellite imagery (Figure 2). Transfer learning in deep learning leverages pre-trained models, which have been trained on large datasets, to capture general features with high accuracy (Pan and Yang., 2009). In this study, we start with a ResNet model pre-trained on the large ImageNet dataset, which comprises over 100 million samples. ResNet, standing for the Residual Network, is a deep convolutional neural network (CNN) architecture that uses skip connections to bypass one or more layers, allowing input data to be added directly to the output (He et al., 2016). These skip connections help mitigate the vanishing or exploding gradient problems often encountered in deep networks. ResNet-34 strikes a balance between model depth and computational efficiency, making it an idea choice for fine-grained mapping tasks (Robinson et al., 2017; Shi et al., 2022) while offering a good trade-off between model capacity and accuracy (Russakovsky et al., 2015).

For the purpose of this study, we modify the first convolutional layer to accommodate our satellite slice inputs, and the last layer to produce a continuous estimate instead of a classification. Specifically, we initialize the RGB channels with weights pre-trained on ImageNet, while for non-RGB channels, we use the average of weights for RGB weights for initialization.~~,~~ ~~scaling all~~ All weights are scaled by a factor of 3/7. Following Yeh et al., (2020), the remaining layers of the ResNet are initialized to their ImageNet values, and the weights for the final layer are initialized randomly. The model is trained using Adam optimizer (Kingma and Ba, 2014) and a mean squared-error loss function with L_2 regularization. The models are trained for 120 epochs, with early stopping implemented to prevent overfitting. The hyperparameter learning rate and L_2 weight regularization are ranged among 0.1, 0.01, 0.001 and 0.0001, and 1, 0.1, 0.01 and 0.001, respectively. After fine-tuning the ResNet-34 model, we leverage it to extract 512-dimensional features from the satellite images. Here we do not incorporate other slum-related geographical characteristics, such as proximity to government agencies or educational facilities, since these quantifications are not sufficiently accurate due to the displacement of cluster locations as indicated in DHS documentations.

Subsequently, we use eXtreme Gradient Boosting tree (XGBoost), a popular and flexible supervised-learning algorithm, to predict the occurrence of slum household in each cluster from 512 features. XGBoost, introduced by Chen and Guestrin (2016), is a scalable machine learning model based on the gradient boosting framework. It builds an ensemble of decision trees by sequentially adding weak learners, each aimed at improving prediction accuracy. The first tree is constructed by splitting features to minimize the loss function, and subsequent trees are generated iteratively, correcting the residuals of previous predictions. This process continues until the stopping criteria are met. In XGBoost, the trees work together to progressively reduce residuals, with the final prediction obtained by aggregating the outputs of all trees. Slums are a visible manifestation of poverty in Global South countries. Reliable estimation of slum population is crucial for urban planning, humanitarian aid provision, and improving well-being. However, large-scale and fine-grained mapping is still lacking due to inconsistent methodologies and definitions across countries. Existing datasets often rely on government statistics, lacking spatial continuity or underestimating slum population due to factors such as city image and privacy concerns. Here, we develop a standardized bottom-up approach to estimate the slum population at the grid-cell level (~6.72 km resolution at the equator) for 129 Global South countries in 2018. Leveraging the Sustainable Development Goals 11.1 framework and machine learning, our estimation integrates household-based surveys, satellite imagery, and grided population data. Our models explain 82% to 96% of the variation in ground-truth surveys, with a root mean squared error of 4.85% to 10.47%, outperforming previous benchmarks. Cross-validation with independent data confirms the reliability of our estimates. To our knowledge, this is the first comprehensive geospatial inventory of slum populations across Global South countries, offering valuable insights for advancing urban sustainability and supporting further research on vulnerable populations. The maps of slum populations and their local shares in Global South countries are available in the Zalando repository at https://doi.org/10.5281/zenodo.13779003 (Li et al., 2025).~~XGBoost is renowned for its high computational efficiency and strong predictive performance, making it particularly suitable for large datasets and high-dimensional feature spacesXGBoost is renowned for its high speed and strong predictive performance, particularly well-suited for large datasets and high-dimensional data (Nielsen, 2016; Ramraj et al., 2016).~~

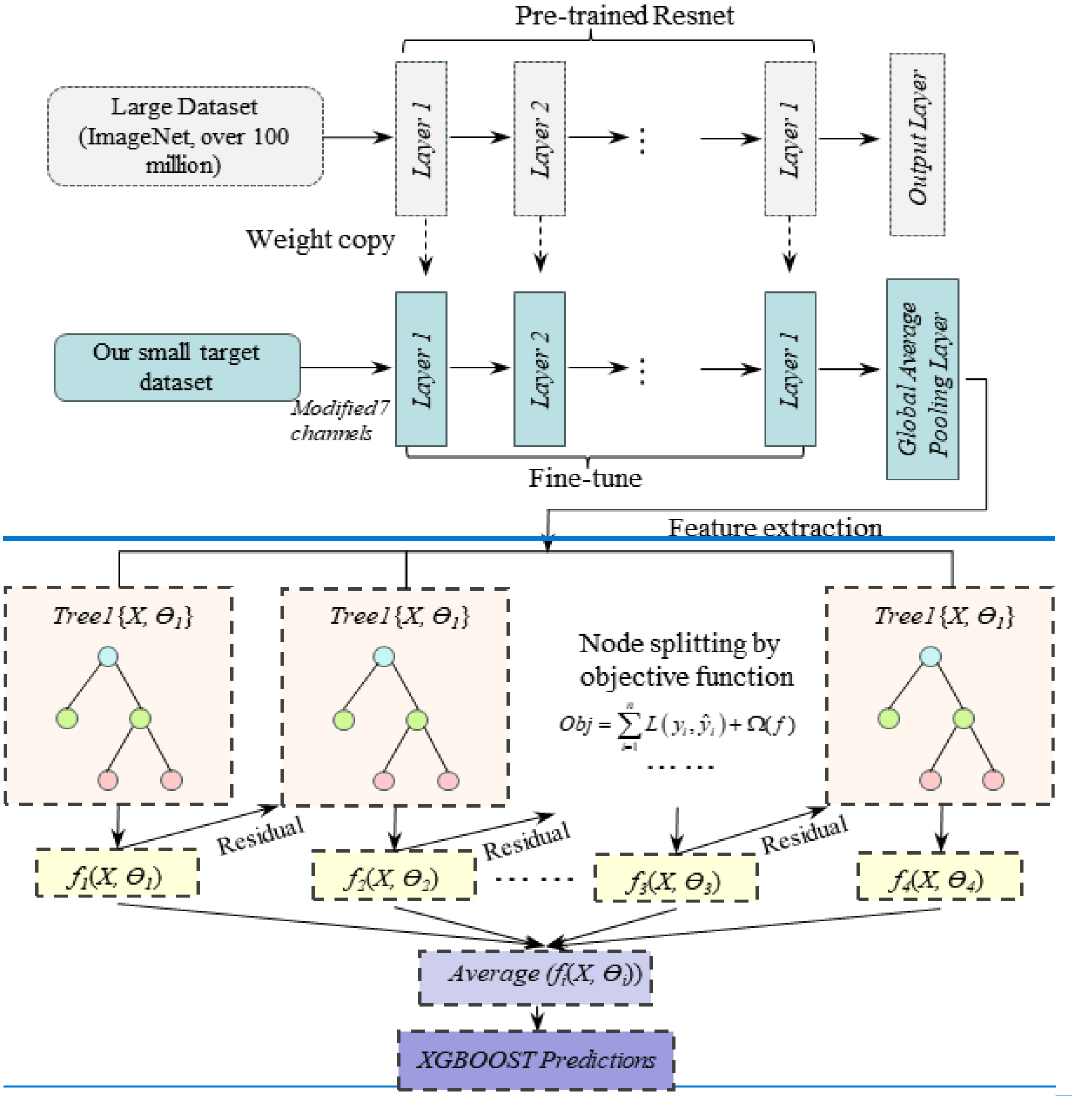

Pre-trained Resnet
Large Dataset (ImageNet, over 100 million)
Layer 1
Layer 2
Layer 1
Output Layer
Weight copy
Our small target dataset
Modified 7 channels
Layer 1
Layer 2
Layer 1
Global Average Pooling Layer
Fine-tune
Feature extraction
Tree1{X, Θ1}
Tree1{X, Θ1}
Node splitting by objective function
$Obj = \sum_{i=1}^{n} L(y_i, \hat{y}_i) + \Omega(f)$
Tree1{X, Θ1}
Residual
Residual
Residual
f1(X, Θ1)
f2(X, Θ2)
f3(X, Θ3)
f4(X, Θ4)
Average (fi(X, Θi))
XGBOOST Predictions

335

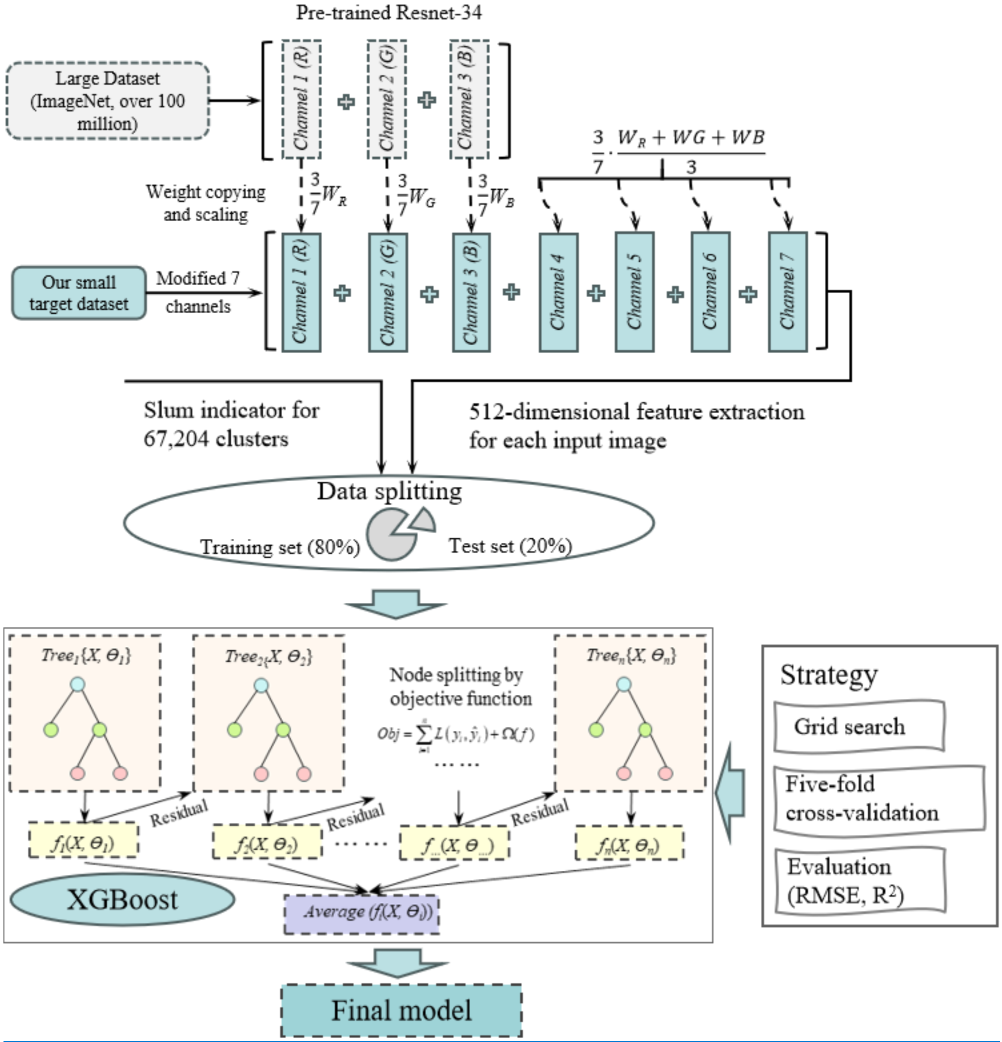

Figure 2 Schematic of the proposed model architecture. It integrates transfer learning by fine-tuning ResNet-34 to extract high-dimensional spatial–spectral features from multispectral imagery, followed by XGBoost regression for predictive modeling. ~~**The model architecture for integrating transfer learning using ResNet-34 as the feature extractor and XGBoost for regression.**~~

~~We perform a grid search to find the optimal combinations of hyperparameters and apply L_2 regularization to the loss function to prevent overfitting. The hyperparameters tuned include the learning rate (learning_rate), the maximum depth of trees (max_depth), the fraction of the training data used for building each tree (subsample), the fraction of features used for each tree (colsample_bytree), the regularization term to control tree complexity (gamma), and the total number of boosting rounds (n_estimators). By optimizing these parameters, we ensure the~~

~~model achieves a balance between predictive performance and generalization. These optimal hyperparameters are then applied to retrain the model on the entire dataset, producing the final model for out-of-sample estimation. Table 3 lists the candidate values considered during the grid search.~~

~~**Table 3 The hyperparameters used in grid search**~~

3.3 Model training, ~~and~~ cross validation and testing

During the model training and cross validation phases, we divide the 53 countries with the DHS data into 9 groups based on their geographical regions and income levels (Table S3). The classification of countries by income level follows the definitions provided by the World Bank (World bank, 2022). In other words, we train nine separate regional models, following the flowchart in Figure 1. To enhance the generalization ability of the models, we group countries for training and validation rather than training individual country-specific models, ensuring a sufficient number of samples per group. While our primary focus is on regional models, we also compare their performance against country-specific models to evaluate potential differences.

We split the spatial-temporal matched satellite images and DHS survey labels into training, validation, and test sets. Specifically, 20% of the dataset is held out as an independent test set to assess the final model's performance, while the remaining 80% is used for training and validation. For robust model evaluation, we employ 5-fold spatially stratified cross-validation. In each fold, the data is divided to maintain equal proportions of urban and rural samples, as well as consistent proportions of samples from each country within the group. During cross-validation, the model is trained on four folds and validated on the remaining fold, repeating the process five times so each fold serves as the validation set once. This rigorous approach enables accurate assessment of the model's generalization ability across different geographic regions and income levels, while ensuring an unbiased evaluation on the held-out test set.

We perform a grid search to identify the optimal combinations of hyperparameters and apply L2 regularization to the loss function to prevent overfitting. The tuned hyperparameters include the learning rate (learning_rate), maximum tree depth (max_depth), fraction of training data used for building each tree (subsample), fraction of features per tree (colsample_bytree), regularization term controlling tree complexity (gamma), and number of boosting rounds (n_estimators). Table 3 lists the candidate values considered. For each hyperparameter combination, we conduct 5-fold cross-validation to train the models and compute average validation performance. The combination with the highest average performance is selected as optimal. We then retrain the model on the entire training and validation dataset using these optimal hyperparameters to update its weight parameters. The final model is evaluated on the hold-out test set to assess generalization. All training, cross-validation, and testing steps are conducted independently for each of the nine regional groups, following the defined data partitioning scheme, yielding nine distinct final regional models~~We perform a grid search to find the optimal combinations of hyperparameters and apply L_2 regularization to the loss function to prevent overfitting. The hyperparameters tuned include the learning rate (learning_rate), the maximum depth of trees (max_depth), the fraction of the training data used for building each tree (subsample), the fraction of features used for each tree (colsample_bytree), the regularization term to control tree complexity (gamma), and the total number of boosting rounds (n_estimators). By optimizing these parameters, we ensure the model achieves a balance between predictive performance and generalization.~~.

~~These optimal hyperparameters are then applied to retrain the model on the entire dataset, producing the final model for out-of-sample estimation. Table 3 lists the candidate values considered during the grid search.~~

Table 3 Hyperparameters used in the grid search for optimizing the XGBoost model. Param_grid indicates the ranges of values explored for each hyperparameter. Best_num_boost_rounds denotes the number of boosting iterations that achieved the highest validation performance.

Hyperparameters	Param_grid
learning_rate	[0.01, 0.03, 0.05, 0.1]
max_depth	[3, 5, 6, 7]
subsample	[0.6, 0.8, 1.0]
colsample_bytree	[0.6, 0.8, 1.0]
gamma	[0, 0.1, 0.2, 0.3]
n_estimators	[best_num_boost_rounds]

3.4 Out-of-samples predictions

Using our final models, we predict slum indicators at the grid-cell level across 129 countries in the Global South. Collected satellite imagery and nighttime light data are first divided into 224×224 pixel slices. The GHS-SMOD and CGLS-LC100 datasets are then applied as spatial masks to classify urban, suburban and rural areas, and to exclude grid-cells dominated by bare ground or sparse vegetation. Based on population estimates from the GHS-POP dataset, any image slice covering an area with a total population below 1,000 people is excluded to avoid unreliable out-of-sample predictions.

The remaining image slices are processed by fine-tuned ResNet-34 models to extract 512-dimensional features, which are subsequently passed to the final regional XGBoost models to generate slum indicator predictions for each 6.72 km grid cell. ~~Using our final models,~~ All auxiliary datasets are resampled to match the 6.72 km spatial resolution of the predicted grid cells. The GHS-POP raster is aggregated by summing adjacent cells to match the approximate scale of the target grid, and then resampled to a 6.72km grid using cubic convolution, with snapping applied to ensure alignment with the predicted slum indicator map. Categorical datasets (GHS-SMOD and CGLS-LC100) are resampled using nearest-neighbor interpolation to retain categorical integrity. All datasets are projected to WGS 1984 for spatial consistency.~~we apply satellite imagery and nighttime light data to grid cells of 6.72-km in Global South countries, focusing on cells with populations exceeding 1,000. This allows us to estimate the cluster-level slum indicators~~

~~across 129 Global south countries, based on the list of the United Nations' Finance Center for South-South Cooperation. Clusters with populations below 1000 are excluded to avoid unreliable out-of-sample estimates.~~

To produce the final map of population living in slums or slum-like conditions, we integrate the GHS-POP dataset with the predicted slum indicator map. In the absence of household-level population statistics at the grid-cell level, we assume that slum and non-slum households have equal average household sizes within each 6.72-km grid cell. Under this assumption, the proportion of slum households corresponds to the proportion of the population living in slums or slum-like conditions. Accordingly, the resampled and spatially aligned GHS-POP population data are multiplies by the predicted slum indicator values to generate the final grid-cell-level map of slum populations.~~To produce the final map of population living in slums or slum-like conditions, we integrate the GHS-POP dataset with the map of cluster-level slum indicator. The slum indicator is used to clip the GHS-pop population grid, and to re-sample the population data for achieving spatial alignment. By combining the slum prevalence map with grided population dataset, we produce the final map of slum population at the cluster-level.~~

We further analyze the local shares of slum population in Global South countries at a resolution of 6.72km. This metric enables cross-country and cross-regional comparisons while accounting for differences in population size. To capture the degree to which local populations lack adequate infrastructure and housing, we implement a hierarchical classification of slum population share, ranging from very low to very high concentration. Specifically, concentration levels are defined by the proportion of the slum population within each grid cell: very low (< 10%), low (10%-20%), moderate (20%-40%), high (40%-60%) and very high (> 60%).

3.~~6~~ 5 Evaluation approaches and robustness analysis

Our slum population framework integrates multiple data sources, making robustness and uncertainty assessment complex. To address this, we adopt a step-by-step evaluation process, which involves validating results from intermediate steps and comparing results with other statistics (Haberl et al., 2021). First, ~~W~~we evaluate model performance using two metrics: the coefficient of determination (R2) and root mean squared error (RMSE). The household-based slum indicator calculated from DHS data serves as the ground truth, while our method generates the predicted slum household indicators.~~e evaluate the performance of the final models using two metrics including coefficient of determination (R^2) and root mean squared error (RMSE).~~ We also compare the performance of our proposed approach with baseline models trained only on RGB (Red, Green, Blue) image bands, in order to assess the added value of using additional image channels. ~~We cross-validate our mapped slum population estimates against a broad range of literature and statistical data at regional, national, and local scales. This comparison provides an additional layer of validation, helping to evaluate the consistency of our estimates with existing data.~~

Second,

~~To test the robustness of our framework,~~ we test the robustness of our framework by evaluat~~e~~ing the model performance~~s~~ under two alternative weighting schemes for the slum indicator: the “Basic Service” scenario and the “UN-Habitat” scenario. In the Basic Service scenario, greater emphasis is placed on water and sanitation, and energy services, with weights of 0.2, 0.4, and 0.4, respectively (Fu et al., 2019). In contrast, the UN-Habitat scenario prioritizes housing and water and sanitation services, assigning weights of 0.4, 0.4, and 0.2 (Mwaniki and Ndugwa, 2021). We then calculate the percentage change in slum population estimates by aggregating the grid-level predictions to the country level, and computing the percentage difference between each alternative scheme and the equal-weight scenario. This sensitivity analysis helps determine how different weighting schemes affect the final predictions.~~–~~ Third, we also compare the performance of regional models with country-specific models, which are all constructed using the equal-weight scenario (0.33, 0.33, 0.33), to identify the strengths and limitations of applying a generalized model across different region/income groups.~~We also compare the performance of regional models with country-specific models to identify the strengths and limitations of applying a generalized model across different geographical areas.~~

Finally, ~~W~~we cross-validate our mapped slum population estimates against a broad range of literature and statistical data at regional, national, and local scales. This comparison provides an additional layer of validation, helping to evaluate the consistency of our estimates with existing data.

4 Results

4.1 Model performance

~~To evaluate the performance of our regional models, we use two metrics, RMSE and R^2, to assess the predictive accuracy of the slum indicator at the cluster level in Africa, Asia, and Latin American regions, respectively (Table 4 and Figure 3). The optimal hyperparameters for the regional models are provided in Table S4. The household-based slum indicator calculated from DHS data serves as the ground truth, while our method generates the predicted values.~~

O~~Overall, o~~ur regional models demonstrate strong performance in predicting the slum household indicators (Table 4 and Figure 3), with RMSE values ranging from 5.20% to 10.17% and R^2 values between 0.82 and 0.95. ~~–~~Specifically, the models achieve an average RMSE of 5.89% in Africa, 6.66% in Asia, and 8.26% in Latin America. The optimal hyperparameters for the regional models are provided in Table S4. This performance may be attributed to the availability of labeled training data from household surveys used during the modeling process. When comparing performance across income groups, models developed for low-income and low-middle-income groups perform better than those for upper-middle-income and high-income groups in Asia and Latin America. It is worth noting that all models deliver satisfactory results.

In Figure 3, scatter points represent the distribution of true versus predicted values, and their even scatter around the 1:1 line indicates no significant overestimation or underestimation. ~~Collectively, the results demonstrate the effectiveness of state-of-the-art machine learning models in capturing the complex relationships between satellite imagery and slum indicators. Given that local household survey data are not always available, our method offers a valuable approach for using limited data to identify the spatial distribution of slum households—a key indicator for estimating affordable and adequate housing, in alignment with SDG 11.1.~~

Table 4 Model performance of slum indicator in Global South

Region/Income Group~~Income groups~~	Model	RMSE (%)	R^2
West Africa – Low Income~~Low income~~	Model 1	5.29	0.93
East Africa – Low Income	Model 2	5.88	0.89
West Africa – Lower middle income~~Lower middle income~~	Model 3	6.40	0.92
East Africa – Lower middle income	Model 4	6.00	0.95
Africa – Upper middle income~~Upper middle income~~	Model 5	8.92	0.83
West Asia – Lower middle income~~Lower middle income~~	Model 6	5.20	0.84
East Asia – Lower middle income~~Lower middle income~~	Model 7	5.87	0.89
Latin American – Lower middle and low income~~Lower- middle and low income~~	Model 8	6.36	0.89
Latin American – High and upper middle income~~High and upper middle income~~	Model 9	10.17	0.82

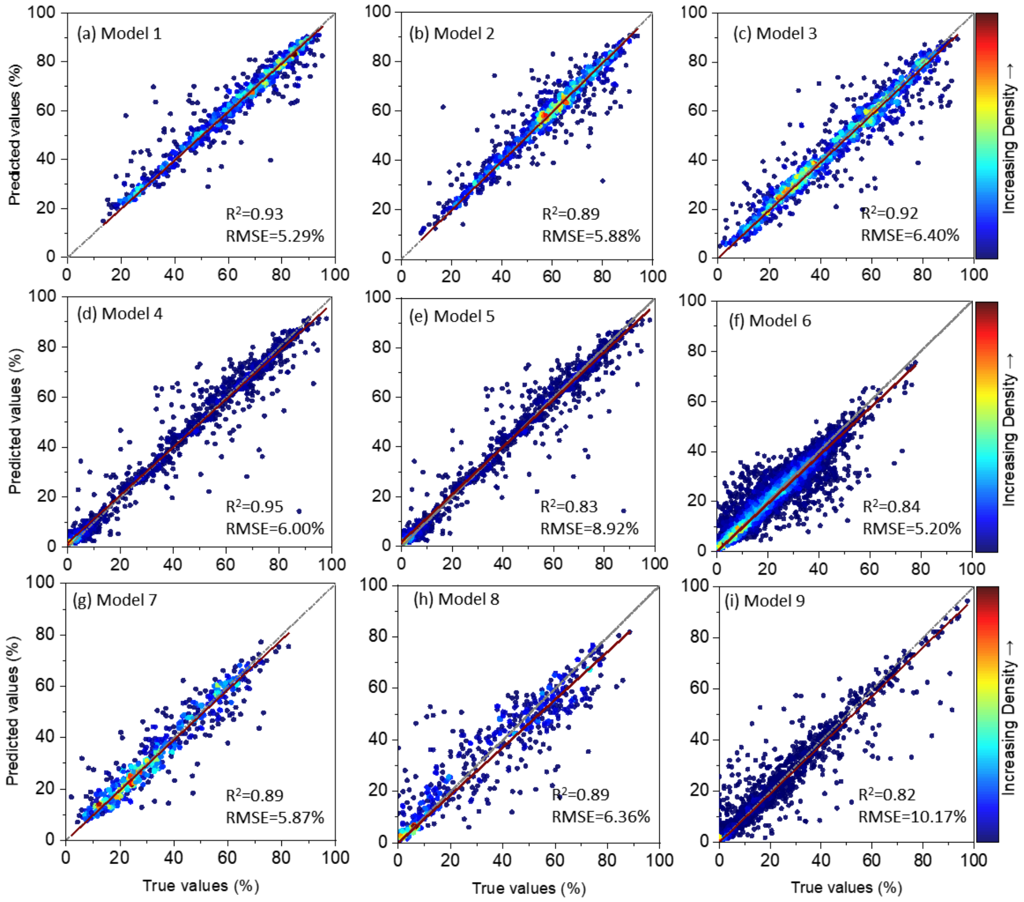

Figure 3 Model performances across different geographical regions and income groups. The true values represent the slum indicator calculated from DHS data using our slum framework, while the predicted values are produced by our machine learning-based models. For each model, a linear regression line is displayed alongside a reference line with a slope of one for comparison.

4.2 Spatially explicit estimates of slum population in Global South

We apply the proposed framework to map slum population in 2018 across 129 Global South countries, including 54 in Africa, 42 in Asia and 33 in Latin America, using a spatial resolution of ~~3.63 arc-minutes (~~6.72 km ~~on~~ at the equator~~)~~. The map is based on 6.72 km grid cells intersecting built-up areas with populations exceeding 1,000, in alignment with the urban-rural delineations provided by the Global Human Settlement Layer~~The map is based on settlement slices, each having a population of over 1,000, and aligns with the delineations of urban and rural areas provided by the Global Human Settlement Layer~~. ~~To refine the analysis, we also use the higher-resolution CGLS-LC100 dataset to mask out other land cover types from the settlement slices.~~

Figure 4a shows the spatial distribution of slum population across Global South countries. In terms of absolute numbers, slum population is concentrated in areas with expected high population densities, such as northern India in Asia, Rwanda and northern Morocco in Africa, and the coastal regions of Rio De Janeiro in Latin America, highlighted in dark blue on the map. Notably, more than 50% of the total slum population resides in less than 8% of the total grid cells.

Figure 4b highlights the administrative statistics and geographic disparities in slum population distribution. At the regional level, we estimate a total of over 0.88 billion people living in slums across the Global South. More than 60% of this population resides in South Asia and Sub-Saharan Africa, followed by East Asia and the Pacific (16%), the Middle East and North Africa (8.6%), Latin America and the Caribbean (7.4%), and Europe and Central Asia (1.7%).

When comparing urban slum populations to those living in slum-like conditions in rural areas, distinct urban-rural differences in settlement patterns emerge. In Latin America and the Caribbean, the Middle East and North Africa, Europe and Central Asia, and East Asia and the Pacific, a higher proportion of the slum population—between 46% and 60%—is concentrated in urban areas. In contrast, 41% of the slum population in South Asia is located in suburban areas, while 44% of those in Sub-Saharan Africa live in rural regions with slum-like conditions and inadequate services.

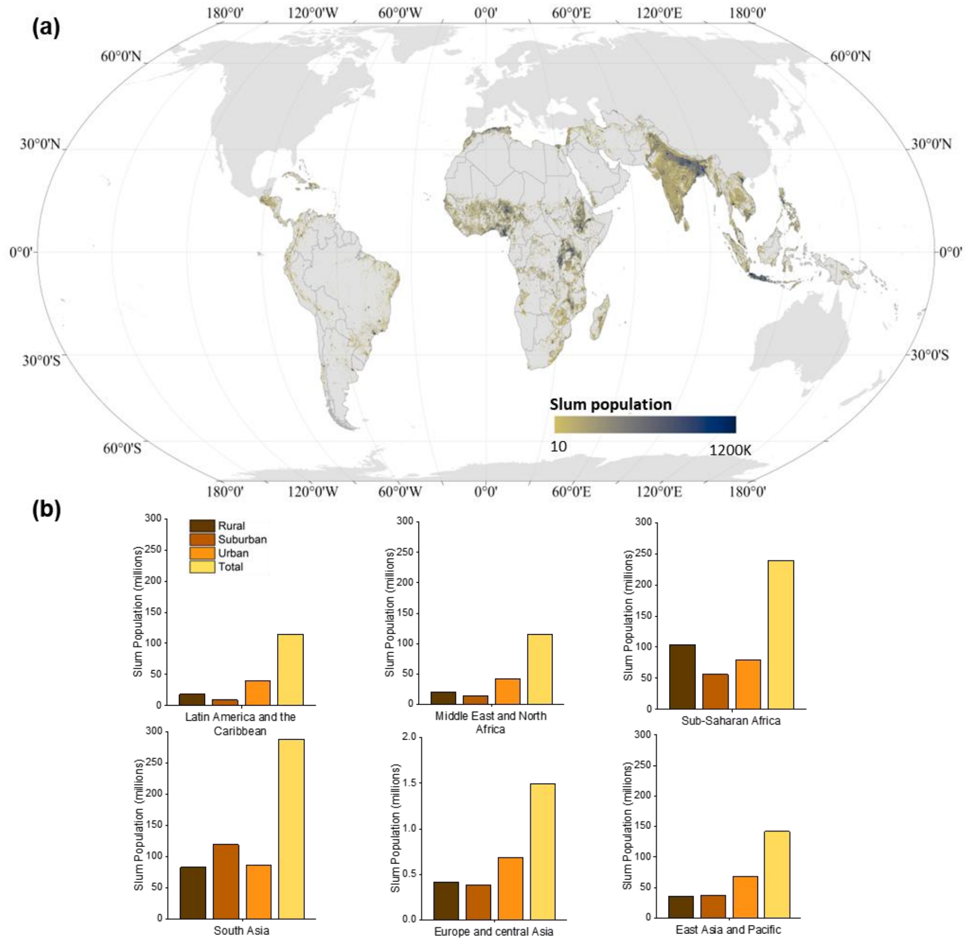

Figure 4 Spatial distribution of slum population in the Global South and their geographic disparities. (a) Map of slum population with a resolution of 6.72km~~3.63 arc-minutes~~. The ~~settlement slice~~grid cells with a population of less than 1,000 are not included. (b) Statistics of slum population across geographic regions and disparities between rural and urban areas.

4.3 Mapping of local shares of slum population in Global South

~~We further estimate the local shares of slum population in Global South countries at a resolution of 3.63 arcminutes (Figure 5). These local shares allow for comparisons across countries and regions, accounting for differences in population sizes. Moreover, we implement a hierarchical classification of slum clusters, ranging from very low to very high concentrated levels, to reflect the extent to which local populations lack adequate infrastructure and housing within a community.~~

As shown in Figure 5a, the spatial distribution of local shares provides new insights into the settlement pattern of slum population. For example, Sub-Saharan Africa exhibits notably high local shares of slum population, with 57% of the local population living in slum conditions. Within this region, countries like Libya and Nigeria show even higher local shares, reaching 70%. Comparatively, Latin America and Caribbean, South Asia, and East Asia have local slum population shares of 28%, 21% and 39%, respectively. Even in smaller countries such as Sierra Leone, the proportion of the population living in slums remains significant, at 60%.

We also analyze the concentration levels of slum ~~clusters~~populations, from very low to very high, across income groups and regional groups (Figure 5b). Across the Global South, about 24% of the slum population resides in very highly concentrated slum ~~clusters~~areas. In low-income countries, 60% of the slum population lives in ~~clusters~~ areas with very high concentration levels. In contrast, slum populations in high-income countries are less concentrated, with 45% living in moderately concentrated ~~clusters~~areas. From a geographic perspective, Sub-Saharan Africa has the highest concentration, with 55% of the slum population living in very highly concentrated ~~clusters~~areas. In other regions, slum populations are mainly concentrated at low or moderate levels. Figure 6 shows visual comparisons between estimated slum population distribution and conditions observed in Google Earth imagery for four representative Global South Cities. The resulting maps show consistent spatial correspondence between areas with high estimated slum populations and known locations of dense slums areas or informal settlements, supporting the reliability of our mapping results.

~~The differing patterns of slum population concentration across Global South countries can be attributed to factors such as urbanization and uneven socioeconomic development. Our map provides rich spatial details on slum populations, both in terms of absolute numbers and local shares, making it a valuable tool for urban planning and slum upgrading initiatives.~~

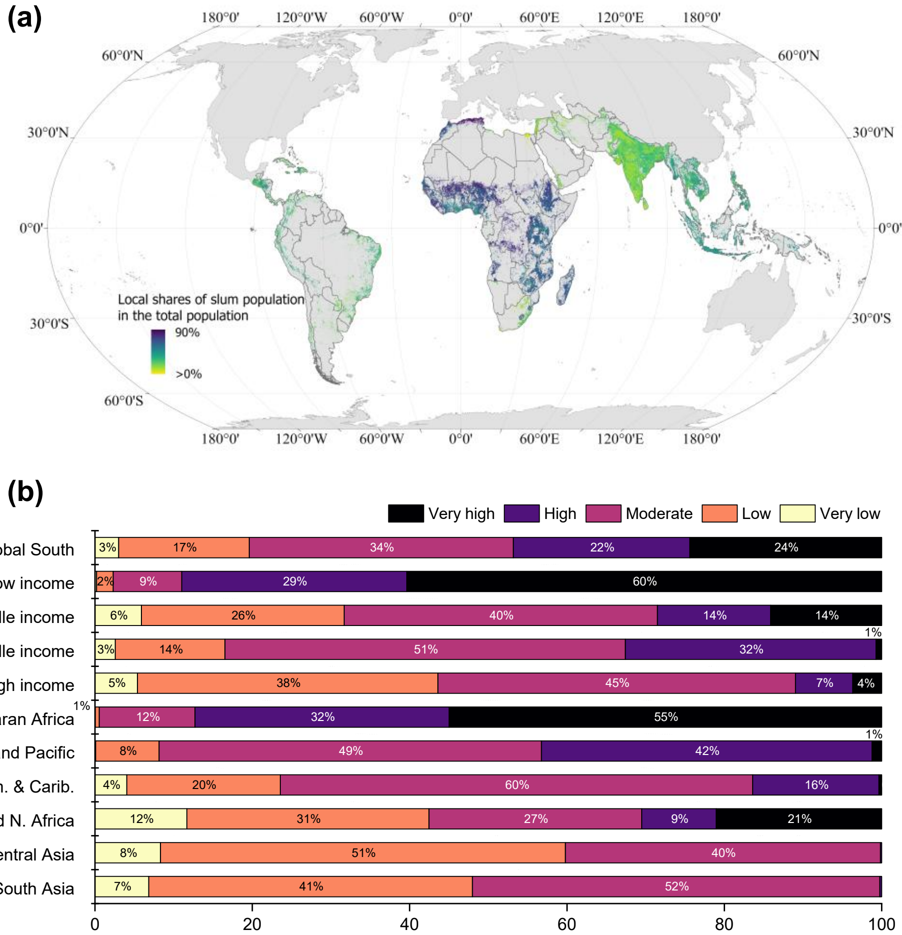

Figure 5 Slum populations categorized by concentration levels, ranging from very low to very high, and their geographic and socioeconomic disparities. (a) Map displaying local shares of the slum population at a resolution of 6.72km~~3.63 arcminutes~~. (b) Statistical analysis of disparities in slum population concentration across different regional and income groups. Concentration levels are classified based on the proportion of the slum population within each grid cell: very low (less than 10%), low (10%-20%), moderate (20%-40%), high (40%-60%) and very high (over 60%).

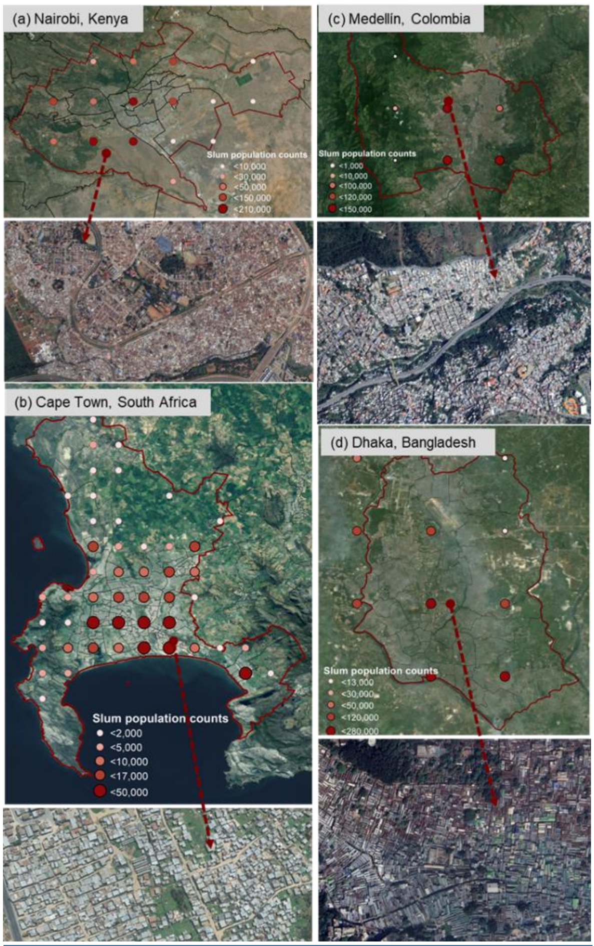

Figure 6. Showcases of visual comparisons between estimated slum population distribution and conditions observed in Google Earth imagery for four representative Global South Cities: (a) Nairobi, Kenya, (b) Cape Town, South Africa, (c) Medellín, Colombia, and (d) Dhaka, Bangladesh. Estimated population counts are shown as circular markers overlaid on Landsat basemaps, with each marker representing a 6.72 km × 6.72 km grid cell. Red arrows indicate locations where high estimated slum populations align with visible informal settlements in Google Earth, providing visual validation of the product.

4.4 Robustness of our regional models

Table 5 reports the performance of nine regional models trained exclusively on RGB image bands. Across all regions, the RGB-only models consistently underperform relative to the 7-band models used in our main approach. On average, RGB-only models exhibit a 6.81-unit higher RMSE and a 0.34 lower R^2, indicating both reduced predictive accuracy and weaker model fit. The performance gap is particularly pronounced in regions such as West Africa and East Asia. These findings illustrate the limitations of relying solely on visible spectrum data for capturing slum-related features and underscore the value of incorporating additional spectral channels such as near-infrared and shortwave infrared to improve model robustness and predictive power.

Table 5 Regional model performance using only RGB image bands. ΔR^2 and ΔRMSE are the differences in model performance between the 7-band models and the RGB-only models.

Region/Income Group	Model	RMSE (%)	R^2	ΔRMSE (%)	ΔR^2
West Africa – Low Income	Model 1	12.98	0.58	-7.69	0.35
East Africa – Low Income	Model 2	12.65	0.53	-6.77	0.36
West Africa – Lower middle income	Model 3	15.00	0.52	-8.60	0.40
East Africa – Lower middle income	Model 4	14.51	0.75	-8.51	0.20
Africa – Upper middle income	Model 5	14.78	0.52	-5.86	0.31
West Asia – Lower middle income	Model 6	10.29	0.41	-5.09	0.43
East Asia – Lower middle income	Model 7	13.34	0.45	-7.47	0.44
Latin American – Lower middle and low income	Model 8	13.99	0.63	-7.63	0.26
Latin American – High and upper middle income	Model 9	13.84	0.49	-3.67	0.33

Figure 7a and 7b illustrate the percentage change in the country-level slum population estimates by comparing the equal weight scenario with two alternative weighting schemes (Section 3.6). We observe that, in both the basic services and UN-Habitat weight scenarios, the percentage change in slum population estimates for most countries in Africa and South Asia, and Brazil in Latin America remains within ±5%. However, in Southeast Asia and other Latin American countries, the percentage change varies from 5% to 10% under the basic service scenario and from -5% to -10% under the UN-Habitat scenario. This suggests that the basic services scenario tends to overestimate slum populations, while the UN-Habitat scenario tends to underestimate them. This means that the equal-weight scenario offers a balanced approach, avoiding the overestimations and underestimations observed in other scenarios. The three maps of slum population distribution under these three weight scenarios are provided in Figure S4.

Figure ~~6~~7c and ~~6~~7d compare the performance of regional models with individual country-specific models. The full list of individual model performance can be found in Table S5.

While the regional models show slightly lower performance in terms of RMSE and R^2 compared to single-country models, the differences are minimal and within a comparable range. This indicates that our regional models achieve both high accuracy and strong generalization ability.

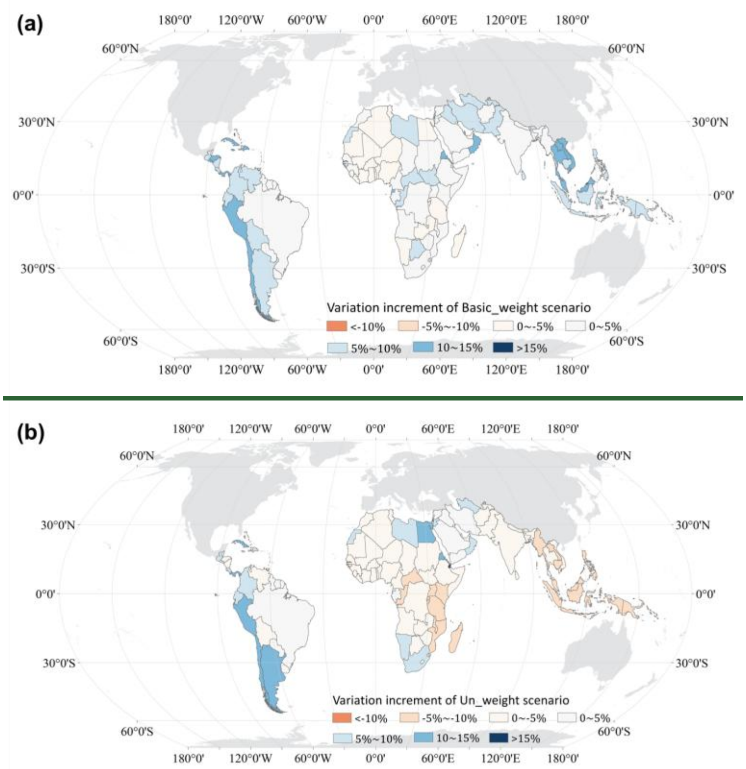
(a)
Variation increment of Basic_weight scenario
<-10%
-5%~-10%
0~-5%
0~5%
5%~10%
10~15%
>15%
(b)
Variation increment of Un_weight scenario
<-10%
-5%~-10%
0~-5%
0~5%
5%~10%
10~15%
>15%

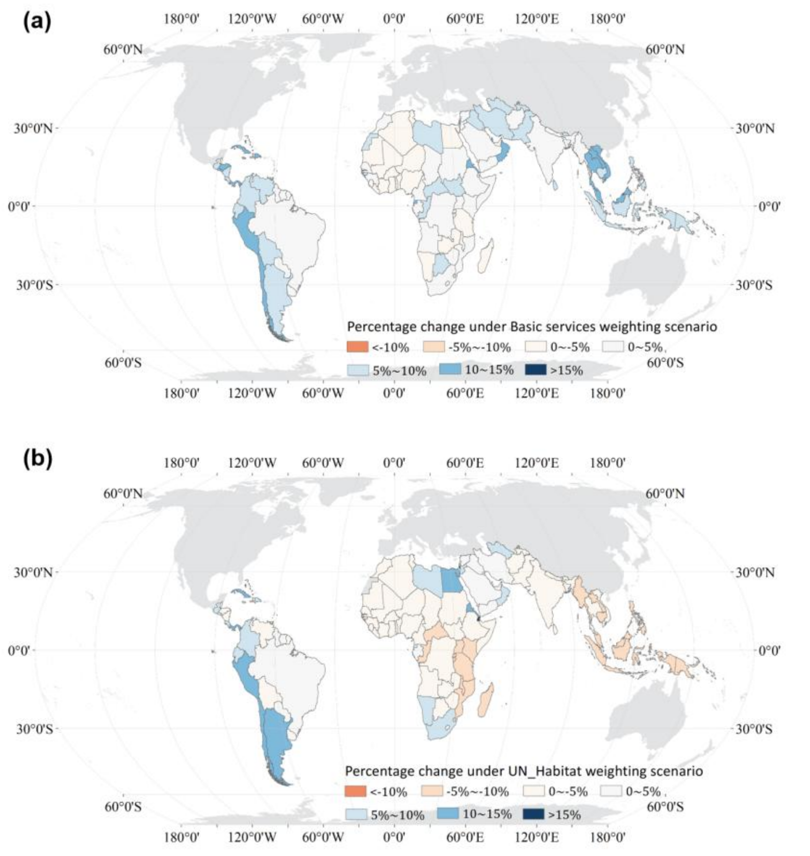
(a)
Percentage change under Basic services weighting scenario
<-10%
-5%~-10%
0~-5%
0~5%
5%~10%
10~15%
>15%
(b)
Percentage change under UN_Habitat weighting scenario
<-10%
-5%~-10%
0~-5%
0~5%
5%~10%
10~15%
>15%

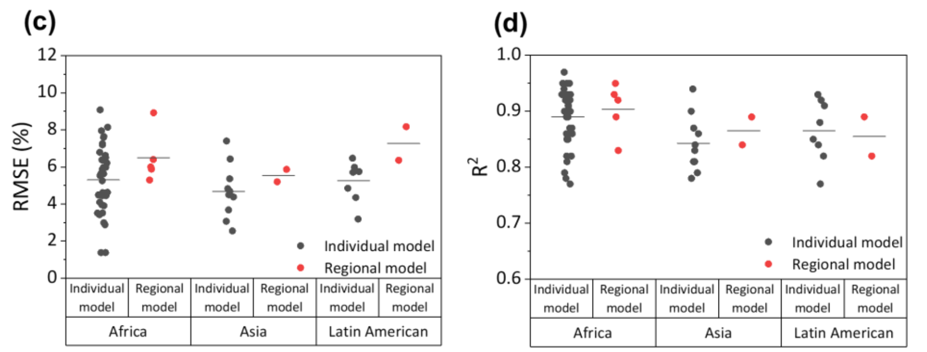

Figure 7 Differences in slum population estimates across two alternative weighting schemes and comparison of model performance between regional models and country-specific models. Panels (a) and (b) show the percentage change in slum population estimates under the Basic Services scenario and the UN-Habitat scenario, respectively. Panels (c) and (d) compare model performance between regional and country-specific individual models using RMSE and R^2 metrics, respectively.~~**Figure 6 Robustness of the slum population framework and generalization ability of our regional models.** Variation in slum population under the basic service (a) and the un-habitat (b) scenarios. Comparison of RMSE (c) and R^2 (d) performance between regional models and country-specific models~~

4.5 Comparison of results with statistical data

We compare our slum population estimates with previous estimates from the literature, which are derived by scaling population counts at individual slum level as well as from city-scale slum population statistics, as summarized in Table 6 (Butera et al., 2019; Byuro, 2015; Davis, 2013; Guilmoto and Rajan, 2013; Medeiros et al., 2012; Patel et al., 2019; Sabry, 2009; Taubenböck and Wurm, 2015). Figure 8a shows our estimates, indicated by an asterisk (*), fall within the range of these scaled slum population estimates. Moreover, when compared to city-scale slum population statistics, our results show strong alignment, particularly in Hyderabad and Johannesburg (Trindade et al., 2021) (Figure 8b). However, for some cities, such as Rio de Janeiro and Dhaka, our results appear to be overestimated. Figure 8c and 8d present a comparison of the relative shares of urban slum populations with the World Bank (2018) and UN-Habitat (2021) statistics. The results show a strong correlation at the national scale (R^2 > 0.95) and good agreement at the regional scale, with an average RMSE of 14% at the national level.

Table 6 Comparison of model-derived slum population estimates with scaled-up figures from sampled slums and published city-level statistics, circa 2015.

City	**Our estimate (million)**	**Scaled-up estimates (million, from sampled slums in other literature)**	**City-level statistics in other literature (million)**	**References**
Rio de Janeiro	3.29	0.96, 1.17, 1.4, 1.46, 1.54, 1.58, 1.91, 2.39, 3.98	2.00	Breuer et al. (2024); Trindade et al. (2021);
São Paulo	2.09	1.3, 1.41, 3.02, 5.67, 8.62	2.16	Breuer et al. (2024); Trindade et al. (2021)
Cape Town	1.45	1.08, 1.13, 1.27, 1.29, 1.38, 1.54, 1.55, 1.89, 2.05, 2.15, 2.2, 2.8	1.23	Breuer et al. (2024)
Cairo	2.56	0.01, 0.3, 0.71, 3.75, 4.55, 7.47	/	Breuer et al. (2024); Sabry (2009);
Mumbai	2.70	1.65, 1.68, 5.2	/	Breuer et al. (2024); Taubenböck and Wurm (2015)
Dhaka	1.85	0.64, 0.76, 1.87, 2.69, 2.73, 3.43, 3.83, 3.84, 4.81, 4.84, 6.61	1.32	Breuer et al. (2024); Patel et al. (2019)
Johannesburg	0.80	/	0.6	Trindade et al. (2021)
Hyderabad	2.28	/	2.3	Trindade et al. (2021)

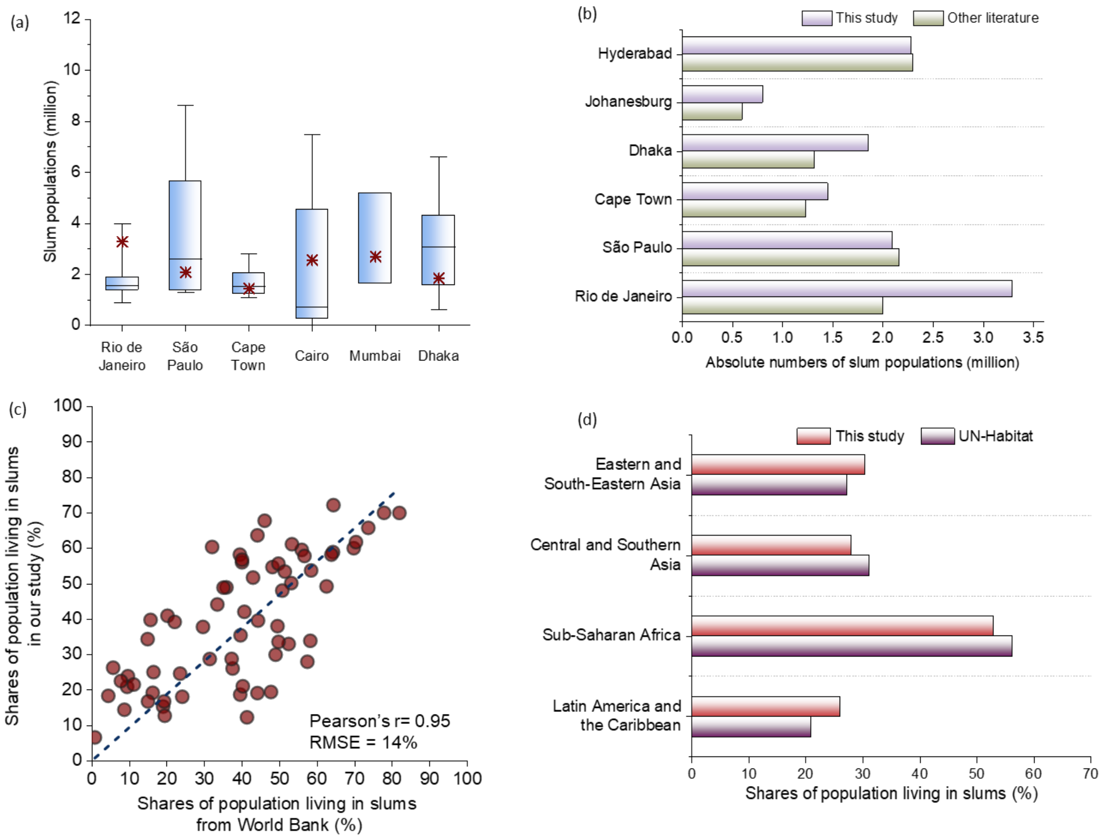

Figure 8 Comparison of our slum population estimates with data from previous literature and official statistics, presented as both absolute numbers and relative

shares. (a) Comparison with scaled-up values from previous studies for six cities: Rio de Janeiro (n=9), São Paulo (n=5), Cape Town (n=12), Cairo (n=6), Mumbai (n=3), and Dhaka (n=11). Scaled-up values are derived by extrapolating slum population counts from multiple sampled slums to the city level. Asterisks indicate estimates from this study. Box plots display the median (central line), interquartile range (box), and minimum-maximum range (whiskers). (b) Comparison with official city-level statistics for the same six cities. (c) Comparison of country-level slum population shares between our estimates and World Bank data; each dot represents a Global South country. (d) Comparison of regional-level slum population shares between our estimates and UN-Habitat data.

5 Discussions

We present a unified, scalable, and operational bottom-up approach for mapping slum populations by~~. Our approach~~ ~~integrates~~ integrating location-specific data, state-of-the-art machine learning, satellite imagery, and population datasets. The model performances demonstrate that such machine learning models are effective in capturing the complex relationships between satellite imagery and slum indicators. Building on this, our ~~This~~ approach enables slum population mapping over large areas~~ and offers the potential to predict slum populations~~ with ~~a~~ high ~~level of~~ spatial details even in countries lacking survey-based data, and allows for cross-compared at both local and regional scales. ~~.~~It facilitates the identification of slum populations—a key indicator for estimating affordable and adequate housing, in alignment with SDG 11.1. ~~The resulting estimates can be cross-compared at both local and regional scales.~~ To the best of our knowledge, this is the first large-scale, spatially explicit inventory of slum populations across the Global South countries.

5.1 Robustness and external validation ~~of our framework~~

Our approach builds on well-established deep learning techniques widely used for mapping poverty, infrastructure access, and progress toward the Sustainable Development Goals (Jean et al., 2016; Chi et al.,2022). We fine-tune the ResNet-34 model on 7-band satellite imagery to more effectively capture the complex spatial-spectral patterns associated with deprived housing conditions. Rather than using ResNet-34 for direct prediction, we extract 512-dimensional embeddings from its penultimate layer and use these as inputs to an XGBoost regression model. This hybrid architecture combines the representational strength of deep CNNs with the predictive robustness of gradient-boosted trees, enabling it to model complex, non-linear relationships in the data.

Slum characteristics vary across countries and regions (da Fonseca Feitosa et al., 2021; do Nascimento et al., 2025), making consistent feature extraction at large spatial scales challenging. We address this systematically across the workflow, from data selection to model design and feature engineering. At the core we adopt transfer learning with Resnet-34 pre-trained on over 100 million ImageNet samples and adapt it to 7-channel multispectral patterns associated with deprived housing conditions. While the original RGB-pretrained ResNet-34 is optimized for general features (e.g., edges and textures), fine-tuning enables early and intermediate filters to learn context-specific cues, such as roof material, settlement density, and vegetation coverage, while leveraging the added information from near-infrared and other bands. The combination of broadly learned representations and increased spectral richness provides a robust foundation for identifying spatial and morphological signatures of slum environments. The approach outperforms RGB-only baseline, highlighting the value of multispectral fine-tuning and high-dimensional feature extraction for modeling housing-related deprivation.

During the model development phase, we constructed regionally stratified models based on geographic location and national income level, rather than separate country-specific models, to improve generalizability and ensure consistent feature extraction across heterogeneous contexts. In addition, the use of publicly available Landsat imagery and DHS ground-truth data provides a uniform, reproducible basis for cross-country analysis. Collectively, these design choices enable consistent and accurate slum feature extraction at scale and underpin the production of a harmonized slum population product. Our regional models demonstrate strong robustness for countries with available training data. ~~Figure 6a and 6b illustrate the percentage change in the country-level slum population estimates by comparing the equal weight scenario with two alternative weighting schemes (Section 3.6). We observe that, in both the basic services and UN-Habitat weight scenarios, the variation in slum population estimates for most countries in Africa and South Asia, and Brazil in Latin America remains within ±5%. However, in Southeast Asia and other Latin American countries, the variation ranges from 5% to 10% under the basic service scenario and from -5% to -10% under the UN-Habitat scenario. This suggests that the basic services scenario tends to overestimate slum populations, while the UN-Habitat scenario~~

~~tends to underestimate them. The three maps of slum population distribution under these three weight scenarios are provided in Figure S4.~~

It is important to note that countries with changes exceeding ±5% are typically regions where nation-wide household-based surveys are not conducted, which is what our machine learning model is trained to estimate. ~~Overall, our regional models demonstrate strong robustness for countries with available training data, although the weighting scenarios have a relatively large impacts on estimates for countries lacking such data. The equal-weight scenario offers a balanced approach, avoiding the overestimations and underestimations observed in other scenarios.~~

Previous studies have addressed slum population underestimation by scaling single-slum estimates to match literature-reported values and then applying these ratios to adjust aggregated population totals (Breuer et al.,2024; Thomson et al., 2021). In contrast, we adopt a direct estimation approach that predicts the proportion of slum households within each enumeration area. First, we operationalize slums from a household perspective by constructing a household-level indicator, expressed as the share of slum households among all households in an enumeration area, and use deep learning to link this indicator directly to features extracted from remote sensing imagery. This design avoids reliance on dichotomous morphological slum maps (which are rarely unavailable at scale) and provides a more flexible, generalizable framework. Second, we use high-quality DHS survey data as labels; their standardized instruments and rigorous quality-control protocols yield valid household-level indicators essential for accurate prediction. Finally, for population distribution, we employ GHS-POP, which refines population estimates along the urban gradient and share a production framework with the GHSL datasets used in this study, thereby reducing uncertainties arising from heterogeneous sources.

Another important consideration for accuracy verification is that external validation datasets may themselves contain uncertainties and limitations, stemming from inconsistent reporting standards, heterogeneous data collection methods, or time lags in statistical updates. To address this, we minimize reliance on any single source by employing a diverse suite of validation data across multiple spatial scales. At the micro level, DHS household surveys provide standardized, representative indicators of slum households based on rigorous sampling. At the meso level, literature-reported estimates and city-level statistics, including both scaled-up values from individual slum areas and directly reported city totals, offer informative reference ranges. At the macro level, national and regional statistics from international organizations such as the World Bank and UN-Habitat provide cross-country benchmarks. Validating against multiple sources and scales strengthens robustness and reduces the risk of bias associated with any single dataset.

~~Figure 6c and 6d compare the performance of regional models with individual country-specific models. To enhance the generalization capabilities of our models, we opt to train regional models rather than individual models for each country. While the regional models show slightly lower performance in terms of RMSE and R^2 compared to single-country models, the differences are minimal and within a comparable range. This indicates that our regional models achieve both high accuracy and strong generalization ability. The full list of individual model performance can be found in Table S5.~~

Given the inherent uncertainty in slum population estimates, we cross-validate our mapping results against a broad range of literature data and government statistical data across multiple scales. Several factors likely contribute to the observed discrepancy. First, our estimates are slightly higher than those reported in the earlier studies. This may be because the slum population figures reported in the literature are from around 2015. Factors such as population growth, migration, and slum upgrading projects may have contributed to changes in slum population over time. Additionally, a recent study indicates that relying solely on the spatial extent of morphological slums and grided population datasets can lead to underestimation of the slum population (Breuer et al., 2024). This evidence supports the advantage of our approach.

Secondly, the definition of slum households in our study does not fully align with those used in the statistical data, which leads to differences in the selection of quantitative indicators. For example, the World Bank's statistics, based on UN-HABITAT definition, adopt a broader perspective that includes housing affordability and security of tenure. Their framework encompasses additional indicators, such as the proportion of households with formal title deeds (to land and housing) and whether a household's monthly net housing expenditure exceeds 30% of their income. Due to data limitations, these specific indicators are not quantified in our study. Instead, we include more detailed sub-indicators, such as access to safely managed drinking water and sanitation services (e.g., households with access to drinking water within a 30-minute round trip), which are absent in the statistical data.

Moreover, the statistical data are compiled from various sources, such as the World Health Surveys (WHS) and Living Standards and Measurement Surveys (LSMS), while our household survey data come from a more singular source. Additionally, in our efforts to generalize a large-scale, unified framework, our regional model estimates for certain countries, especially small island nations, may exhibit bias due to the lack of specific survey data. Further research should focus on refining and validating these estimates, especially when more high-resolution reference datasets and local-scale models become available.

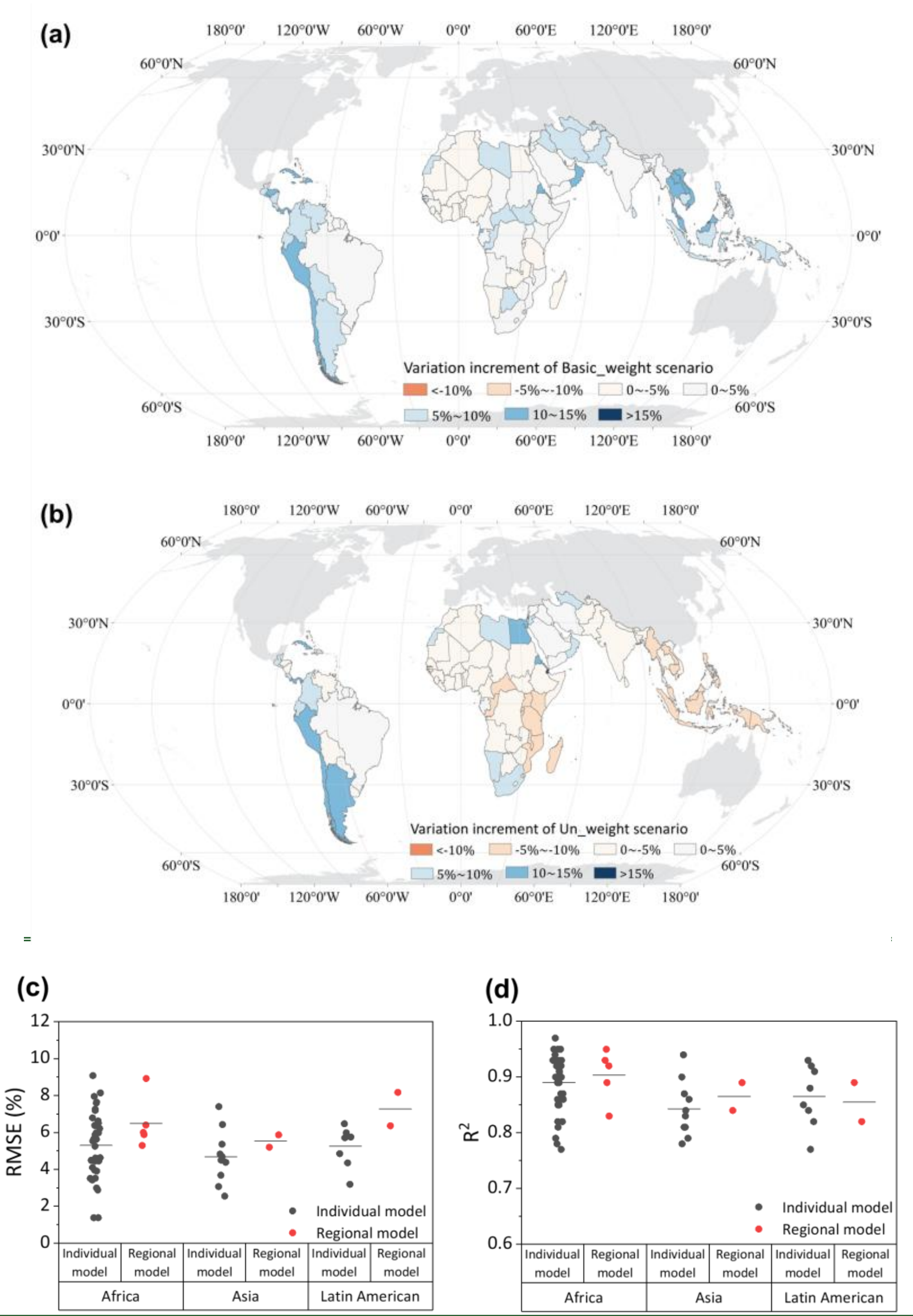

~~**Figure 6 Robustness of the slum population framework and generalization ability of our regional models.** Variation in slum population under the basic service (a) and the un-~~

~~habitat (b) scenarios. Comparison of RMSE (c) and R^2 (d) performance between regional models and country-specific models~~

5.2 Spatial resolution and dataset selection

Our maps of slum population distribution and their local shares are presented at a spatial resolution of 6.72km~~3.63 arcminutes~~. The mapping resolution is primarily determined by the technical requirements of the deep learning architecture and the native spatial resolution of the satellite imagery used. Specifically, the ResNet-34 model for feature extraction requires input images in a 224x224 pixel format~~The ResNet-34 deep learning architecture used for feature extraction requires the input image to be in a 224x224 pixel format~~ (Wu et al., 2019).~~–~~ It is also crucial to ensure spatial and temporal consistency between the satellite images and survey data, which vary across years and countries. To enrich the input feature space, we prioritize images with more spectral bands than standard RGB. Landsat imagery offers consistent temporal coverage, global reach, and multiple spectral bands at 30-meter resolution, making it well suited to our task (Wulder et al., 2022).~~This spatial resolution is carefully chosen based on several factors, including the characteristics of satellite imagery, algorithm architecture, and the truth-ground survey data. It is crucial to ensure spatial and temporal match between satellite images and survey data, given the diverse ranges of household-based survey data collected across multiple years and countries. To enhance input data richness, we prefer satellite images with more spectral bands beyond the standard three RGB bands (Wulder et al., 2022)~~ Based on these considerations, the mapping resolution is set at 6.72 km at the equator.~~, such as Landsat imagery, which offers consistent temporal coverage, global reach, and multiple spectral bands, with a resolution of 30 meters.~~

~~The ResNet-34 deep learning architecture used for feature extraction requires the input image to be in a 224x224 pixel format (Wu et al., 2019). Consequently, the resolution of our maps is set at 3.63 arcminutes (6.72 km on equator) to balance these technical requirements.~~ This resolution aligns with other published maps that focus on sub-dimensions of poverty, such as the wealth index and education (Local Burden of Disease Educational Attainment Collaborators, 2020; Yeh et al., 2020), and provides more granular local insights beyond the administrative boundaries typically used in slum population statistics

(Tjia and Coetzee, 2022). While our method relies on slum proxy ~~at the~~for each cluster ~~level~~ rather than precise slum boundaries, it nonetheless yields valuable insights for large-scale. cross-national estimates of slum populations under current data constraints. Although this resolution does not capture the fine-grained morphology of slums, it effectively identifying populations living in slum-like conditions. Future research can build on this foundation by producing higher-resolution slum data to address this limitation.

The performance of any machine learning or deep-learning model relies heavily on the quality and suitability of its trained data (Meena et al., 2023). The DHS datasets provide accurate, representative, household-based survey data on demographic and socioeconomic conditions; our samples cover over 1 million households across 67,204 clusters in 53 countries of the Global South~~The quality of any machine learning or deep learning model relies heavily on the data it is trained on (Meena et al., 2023). The DHS datasets provide accurate and representative household-based survey data on population characteristics and socioeconomic factors~~. However, a limitation of this dataset is the intentional perturbation of the latitude and longitude coordinates to protect the privacy of the surveyed households. This perturbation introduces random jitter of 2km in urban areas and 5km in rural areas (Owusu et al., 2021). The 6.72km~~3.63 arcminutes~~ resolution of our maps strikes a balance between preserving privacy, leveraging available data, and ensuring the technological feasibility of our approach.

Grided population data are also critical for measuring and mapping slum populations. Widely used global products, such as GPWv4.11 (CIESIN et al., 2018), GHS-POP (Pesaresi et al., 2016), and World Pop (Stevens et al., 2015), as well as regional/national products like HRSL (Smith et al., 2019), differ markedly in inputs, ancillary datasets, and dasymetric methods for redistributing population to grid cells. While regional products such as HRSL can achieve high accuracy at finer resolutions, their limited spatial coverage impedes large-scale, cross-country comparisons, especially in the Global South. Following the 'fitness-for-use' principle (Juran et al., 1979), we select GHS-POP for its distinctive advantages aligned with our objectives. Because it is grounded in human-settlement information, GHS-POP effectively refines population estimates along the urban gradient, which is critical for slum population modeling. Moreover, the Global Human Settlement Layer (GHSL), which leverages Landsat imagery, aligns with the satellite images used in this study, reducing uncertainties introduced by heterogeneous sources.~~The grided population dataset is also a critical component for measuring and mapping the slum population. Widely used global population datasets, such as GPWv4.11 (CIESIN et al., 2018), GHS-POP (Pesaresi et al., 2016), World Pop (Stevens et al., 2015), and regional/national products like HRSL (Smith et al., 2019), vary significantly in characteristics and assumptions. These differences arise from the nature and heterogeneity of the input population data, the ancillary data involved, and the methodological framework applied to redistribute population counts to grid cells. Although some regional products like HRSL show commendable accuracy in identifying building footprints and population distributions at finer resolutions, their limited coverage poses challenges for large-scale cross-country comparisons, especially in the Global South.~~

~~Considering the 'fitness to use' principle (Juran et al., 1979), the GHS-POP dataset has distinctive advantages closely aligned with our research objectives. Grounded in human settlement information, GHS-POP is effective for spatially refining population data along the urban gradient, making it ideal for our slum population modeling. Additionally, the Global Human Settlement Layer (GHSL), which uses Landsat imagery, aligns with the satellite images used in this study, reducing uncertainties introduced by using different data sources.~~

~~5.3 Comparison of results with statistical data~~

~~Given the inherent uncertainty in slum population estimates, we cross-validate our mapping results against a broad range of literature data and government statistical data across multiple scales. We first compare our slum population estimates with previous estimates from the literature, which are derived by scaling population counts at individual slum level (Butera et al., 2019; Byuro, 2015; Davis, 2013; Guilmoto and Rajan, 2013; Medeiros et al., 2012; Patel et al., 2019; Sabry, 2009; Taubenböck and Wurm, 2015). Our estimates, indicated by an asterisk (*), fall within the range of these scaled slum population estimates (Figure 7a). Moreover, when compared to city-scale slum population statistics, our results show strong alignment, particularly in Hyderabad and Johannesburg (Trindade et al., 2021) (Figure 7b). However, for some cities, such as Rio de Janeiro~~

~~and Dhaka, our results appear to be overestimated. This discrepancy may be because the slum population figures reported in the literature are from around 2015. Factors such as population growth, migration, and slum upgrading projects may have contributed to changes in slum population over time. Additionally, a recent study indicates that relying solely on the spatial extent of morphological slums and grided population datasets can lead to underestimation of the slum population (Breuer et al., 2024). This supports the advantage of our approach.~~

~~A comparison of the relative shares of urban slum populations with the World Bank (2018) and UN-Habitat (2021) statistics shows a strong correlation at the national scale ($R^2 > 0.95$) and good agreement at the regional scale (Figure 7c and 7d), with an average RMSE of 14% at the national level.~~

~~Several factors likely contribute to the observed discrepancy. First, the definition of slum households in our study does not fully align with those used in the statistical data, which leads to differences in the selection of quantitative indicators. For example, the World Bank's statistics, based on UN-HABITAT definition, adopt a broader perspective that includes housing affordability and security of tenure. Their framework encompasses additional indicators, such as the proportion of households with formal title deeds (to land and housing) and whether a household's monthly net housing expenditure exceeds 30% of their income. Due to data limitations, these specific indicators are not quantified in our study. Instead, we include more detailed sub-indicators, such as access to safely managed drinking water and sanitation services (e.g., households with access to drinking water within a 30-minute round trip), which are absent in the statistical data.~~

~~Moreover, the statistical data are compiled from various sources, such as the World Health Surveys (WHS) and Living Standards and Measurement Surveys (LSMS), while our household survey data come from a more singular source. Additionally, in our efforts to generalize a large-scale, unified framework, our regional model estimates for certain countries, especially small island nations, may exhibit bias due to the lack of specific survey data. Further research is needed to refine and validate these results, especially as more high-resolution reference datasets and local-scale models become available in the future.~~

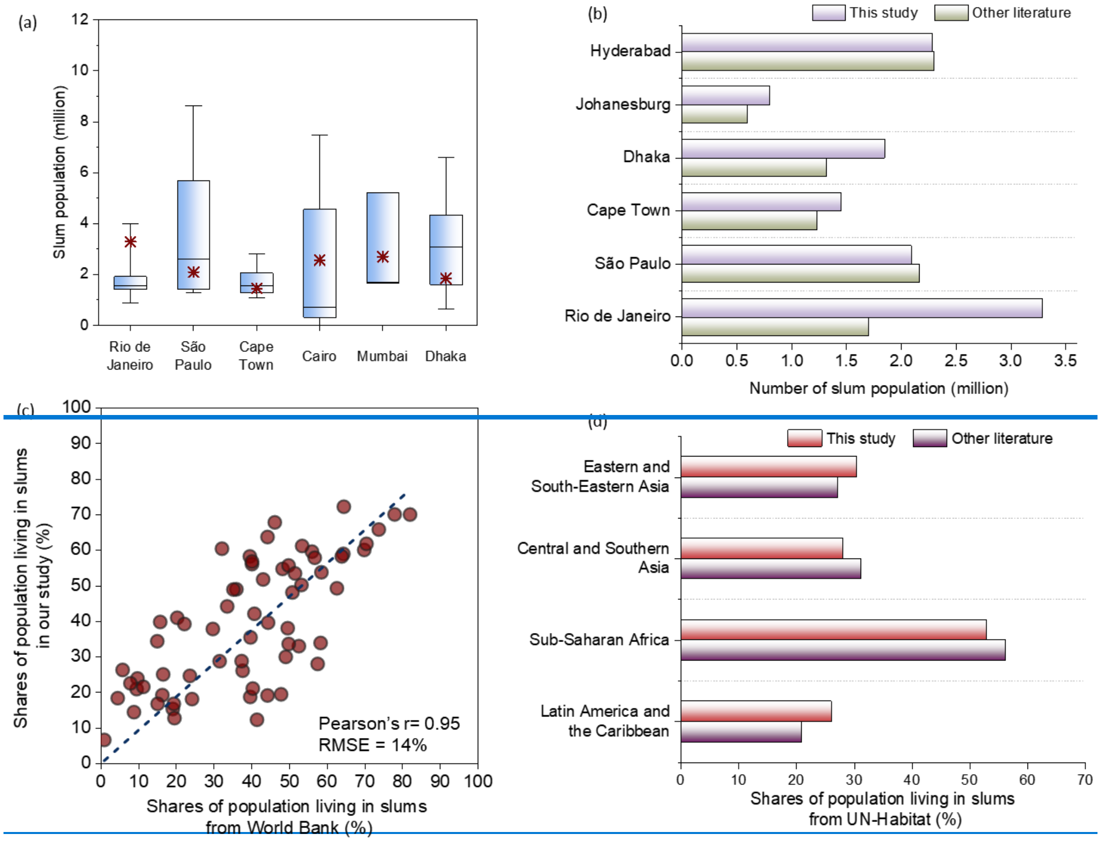

~~**Figure 7 Comparison of our slum population estimates with data from the literature and government statistics, including the absolute numbers and relative shares.**~~

5.~~4~~3 Implications and future research

Our study provides a foundation for generating large-scale, fine-grained slum population estimates, especially in data-sparse environments across Global South countries. The product advances a human-centered mapping framework, prioritizing populations living in inadequate housing rather than focusing solely on the physical delineation of slum settlements. Theoretically, it exposes gaps in progress toward the Sustainable Development Goals by providing spatially continuous, gridded estimates that directly quantify the number of people affected by deficits in water, sanitation, and electricity. These wall-to-wall estimates reveal local variation and spatial gradients that are often obscured by administrative boundaries or survey aggregates. Because the approach does not depend on pre-defined morphological slum boundaries, it supports population estimation in regions lacking boundary data and can be dynamically updated as new datasets become available. ~~First, this inventory reveals the significant gaps in the efforts of these countries to achieve sustainable development goals. Our estimates provide~~

~~compelling evidence to raise awareness among governments and organizations about the scale of the slum issue, advocating for more effective allocation of funds and resources to the areas most in need during the slum upgrading projects.The differing patterns of slum population concentration across Global South countries can be attributed to factors such as urbanization and uneven socioeconomic development. Our map provides rich spatial details on slum populations, both in terms of absolute numbers and local shares, making it a valuable tool for urban planning and slum upgrading initiatives.~~

~~Second, given the overcrowded and unsanitary conditions in slums, which are often associated with waterborne diseases, our maps serve as valuable reference data for addressing environmental issues, health-related challenges, and climate change impacts. Additionally, the data can help policymakers and stakeholders identify slum communities at risk during extreme weather events such as floods or droughts, supporting the planning and implementation of relocation or emergency response strategies.~~

Practically, this continuous representation enables flexible aggregation across multiple spatial scales (e.g., neighborhood, city, national) and provides a robust, data-driven foundation for human-centered urban planning, targeted resource allocation, and evidence-based policy design. For example, planners can optimize the spatial distribution of schools, clinics, and parks to improve accessibility and equity for vulnerable populations, thereby supporting inclusive urban development. These estimates also inform resource allocation and emergency response planning aligned with actual population needs. When combined with spatial information on environmental hazards, such as floods, heat islands, or air pollution, the gridded product becomes a critical tool for resilience planning and adaptive governance, enabling social protection and welfare programs tailored to those at greatest risk.

Our framework is transferable and supports dynamic, temporal analyses of slum populations. It enables forward-looking predictions by leveraging patterns learned from existing datasets in combination with updated Landsat imagery and nighttime lights data. Through data-driven learning, the framework extracts informative features from satellite imagery and captures the relationships between spectral characteristics and slum household proxies, facilitating generalization to new spatial and temporal contexts. To ensure reliable predictions, input satellite datasets must be consistent in resolution and spatial extent, with preprocessing steps such as cloud masking carefully applied. Recalibration using newly released ground-truth survey data is recommended, as these labels provide an empirical benchmark to evaluate model performance and correct biases, particularly in rapidly urbanizing areas where slum populations may change significantly. By integrating spatial and temporal information, the framework provides a flexible and robust tool for rapid monitoring and spatiotemporal prediction in data-scarce and fast-changing contexts.

In this study, we assume that the proportion of slum households is equivalent to the proportion of the population living in slums or slum-like conditions. This is a practical approximation given the lack of the household size statistics at the grid-cell scale. Evidence from the 2011 Indian National Census (Chandramouli, 2011) supports its plausibility, showing minimal differences in household size distribution between urban and slum households. For example, 1-3 member households comprise 29.0% of urban households and 28.1% of slum households, while 6-8 member households account for 20.6% and 22.2%, respectively. Nonetheless, we acknowledge this as a potential limitation. Future work incorporating spatially explicit household size data could further improve the accuracy of slum population estimates.

Overall, our study has broader implications for urban planning, resource allocation, and the improvement of human well-being among slum populations. The insights provided by our maps support evidence-based decision-making and targeted interventions aimed at achieving sustainable development goals. Since our approach is based on free and openly available data, it can be extended over time to track the dynamics of slum populations at the grid-cell ~~cluster~~ level. Multi-temporal slum population maps could help uncover the underlying drivers of slum growth, in addition to the forces of local population growth and migration. With more accurate geospatial survey data and higher-resolution satellite imagery, we anticipate significant improvements in the resolution and accuracy of slum population maps. This progress will greatly enhance our understanding of the distribution and scale of slums, enabling more informed decision-making and more effective interventions.

6 Data availability

The maps of slum populations and their local shares in Global South countries are available in the Zalando repository at https://doi.org/10.5281/zenodo.13779003 (Li et al., 2025). All household-based data are available for downloading, free of charge by registered users, from the DHS Program (https://www.dhsprogram.com/data/), satellite images and land cover layers product are download on GEE platform (https://earthengine.google.com/). Global NPP-VIIRS-like nighttime light dataset is from Chen et al. (~~2020~~2021). The Settlement Model grid (GHS-SMOD) and Population Grid (GHS-POP) can be obtained from Global Human Settlement Layer (https://ghsl.jrc.ec.europa.eu/download.php).

7 Conclusions

In this study, we develop a standardized, operational, and bottom-up framework for producing fine-grained, spatially explicit estimates of slum populations. Our framework is based on SDG 11.1 slum household indicators and combines feature extraction techniques with machine learning algorithms. It integrates household-based surveys, satellite imagery, and grided population data to address the underestimation of slum populations found in prior studies, which often relied heavily on slum geometry. Our approach provides reliable slum population predictions, particularly in data-scarce environments.

The resulting maps represent the first comprehensive inventory of slum populations across Global South countries, produced at a spatial resolution of 6.72km at the equator~~The resulting maps are the first comprehensive inventory of slum populations across Global South countries, created with a spatial resolution of 3.63 arcminutes (6.72km at the equator) to protect privacy~~. The models exhibit strong performance and robustness, achieving RMSE values of 5.20%-10.17% and R^2 values of 0.82-0.95 when validated against slum indicators derived from DHS surveys.~~The models demonstrate strong performance and robustness, with RMSE values ranging from 5.20% to 10.17% and R^2 values between 0.82 and 0.95.~~ Our estimates fall within the range of scaled slum population estimates from existing literature and exhibit strong correlations with them at both national and regional scales. This approach offers a valuable tool for generating reliable slum population estimates, and the dataset produced will support a wide range of evidence-based decision-making and targeted interventions aimed at achieving city-level sustainable development goals.

Author contributions

D.L. designed the research. D.L. developed the model and datasets. L.S. provided guidance on data validation. L.S and D.L. led the drafting of the manuscript. D.L., L.S. Y.Y. and P.T. contributed significantly to the final writing of the article.

Competing interests

The contact author has declared that none of the authors has any competing interests.

Disclaimer

Publisher’s note: Copernicus Publications remains neutral with regard to jurisdictional claims made in the text, published maps, institutional affiliations, or any other geographical representation in this paper.

Acknowledgements

This research was funded by the National Natural Science Foundation of China (72403147), China Postdoctoral Science Foundation (2023M732043), and the Shandong Provincial Natural Science Foundation (ZR2023QG076).

References

Abascal, A., Rothwell, N., Shonowo, A., Thomson, D.R., Elias, P., Elsey, H., Yeboah, G., Kuffer, M. “Domains of deprivation framework” for mapping slums, informal settlements, and other deprived areas in LMICs to improve urban planning and policy: A scoping review. Computers, environment and urban systems 93, 101770, https://doi.org/10.1016/j.compenvurbsys.2022.101770 , 2022.

Angeles, G., Lance, P., Barden-O'Fallon, J., Islam, N., Mahbub, A., Nazem, N.I. The 2005 census and mapping of slums in Bangladesh: design, select results and application. International journal of health geographics 8, 1-19, https://doi.org/10.1186/1476-072x-8-32 , 2009.

Azzari, G., Lobell, D. Landsat-based classification in the cloud: An opportunity for a paradigm shift in land cover monitoring. Remote Sensing of Environment 202, 64-74, https://doi.org/10.1016/j.rse.2017.05.025 , 2017.

Banerjee, A., Banerji, R., Berry, J., Duflo, E., Kannan, H., Mukerji, S., Shotland, M., Walton, M. From proof of concept to scalable policies: Challenges and solutions, with an application. Journal of Economic Perspectives 31, 73-102, https://doi.org/10.1257/jep.31.4.73, 2017.

Baynes, J., Neale, A., Hultgren, T. Improving intelligent dasymetric mapping population density estimates at 30 m resolution for the conterminous United States by excluding uninhabited areas. Earth system science data 14, 2833, https://doi.org/10.5194/essd-14-2833-2022 , 2022.

Binzel, C., Fehr, D. Social distance and trust: Experimental evidence from a slum in Cairo. Journal of Development Economics 103, 99-106, https://doi.org/10.1016/j.jdeveco.2013.01.009 , 2013.

Björkman, L. Becoming a slum: from municipal colony to illegal settlement in liberalization era Mumbai. Contesting the Indian city: global visions and the politics of the local, 208-240, https://doi.org/10.1002/9781118295823.ch8, 2013.

Breuer, J.H., Friesen, J. Methods to assess spatio-temporal changes of slum populations. Cities 143, 104582, https://doi.org/10.1016/j.cities.2023.104582 , 2023.

Breuer, J.H., Friesen, J., Taubenböck, H., Wurm, M., Pelz, P.F. The unseen population: Do we underestimate slum dwellers in cities of the Global South? Habitat International 148, 103056, https://doi.org/10.1016/j.habitatint.2024.103056 , 2024.

Buchhorn, M., Smets, B., Bertels, L., De Roo, B., Lesiv, M., Tsendbazar, N.E., Herold, M. and Fritz, S. Copernicus global land service: land cover 100m: collection 3: epoch 2019: Globe, https://zenodo. org/record/3939050, 2020.

Burgert, C.R., Colston, J., Roy, T., Zachary, B. Geographic displacement procedure and georeferenced data release policy for the Demographic and Health Surveys. Icf International, https://doi.org /10.13140/RG.2.1.4887.6563, 2013.

Burke, M., Driscoll, A., Lobell, D.B., Ermon, S. Using satellite imagery to understand and promote sustainable development. Science 371, eabe8628, https://doi.org/10.1126/science.abe8628 , 2021.

Butera, F.M., Caputo, P., Adhikari, R.S., Mele, R. Energy access in informal settlements. Results of a wide on site survey in Rio De Janeiro. Energy Policy 134, 110943, https://doi.org/10.1016/j.enpol.2019.110943 , 2019.

Byuro, B.P.k.n. Census of slum areas and floating population 2014, http://arks.princeton.edu/ark:/88435/dsp01wm117r42q, 2015.

Center for International Earth Science Information Network (CIESIN), Columbia University. Gridded Population of the World, Version 4 (GPWv4): Population Density, Revision 11. NASA SEDAC. https://doi.org/10.7927/H4F47M65, 2018.

Chandramouli C. Housing stock, amenities and assets in slums-Census 2011. New Delhi: Office of the Registrar General and Census Commissioner; 2011.

Chen Z, Yu B, Yang C, Zhou Y, Qian X, Wang C, Wu B, Wu J. An extended time-series (2000–2018) of global NPP-VIIRS-like nighttime light data from a cross-sensor calibration. Earth System Science Data Discussions, 1-34, https://doi.org/10.5194/essd-13-889-2021 , ~~2020~~2021.

Chen, T. and Guestrin, C. Xgboost: A scalable tree boosting system, Proceedings of the 22nd acm sigkdd international conference on knowledge discovery and data mining, San Francisco, California, USA, 785–794, https://doi.org/10.1145/2939672.2939785 , 2016

Da Fonseca Feitosa, F., Vasconcelos, V. V., de Pinho, C. M. D., da Silva, G. F. G., da Silva Gonçalves, G., Danna, L. C. C., & Lisboa, F. S. (2021). IMMerSe: An integrated methodology for mapping and classifying precarious settlements. Applied geography, 133, 102494.

https://doi.org/10.1016/j.apgeog.2021.102494.

Davis, M. Planet of slums. New Perspectives Quarterly 30, 11-12, https://doi.org/10.1111/npqu.11395, 2013.

Doe, B., Peprah, C., Chidziwisano, J.R. Sustainability of slum upgrading interventions: Perception of low-income households in Malawi and Ghana. Cities 107, 102946, https://doi.org/10.1016/j.cities.2020.102946 , 2020.

Do Nascimento, G.A., Giannotti, M., Regueira, T.A. and Tomasiello, D.B., 2025. Identifying slum areas: A multidimensional analysis leveraging with explanatory machine learning techniques. Sustainable Cities and Society, 131, 106645. https://doi.org/10.1016/j.scs.2025.106645

Elvidge, C.D., Baugh, K., Zhizhin, M., Hsu, F.C., Ghosh, T. VIIRS night-time lights. International journal of remote sensing 38, 5860-5879, https://doi.org/10.1080/01431161.2017.1342050 , 2017.

Engin, Z., van Dijk, J., Lan, T., Longley, P.A., Treleaven, P., Batty, M., Penn, A. Data-driven urban management: Mapping the landscape. Journal of Urban Management 9, 140-150, https://doi.org/10.1016/j.jum.2019.12.001 , 2020.

Ezeh, A., Oyebode, O., Satterthwaite, D., Chen, Y.-F., Ndugwa, R., Sartori, J., Mberu, B., Melendez-Torres, G.J., Haregu, T., Watson, S.I. The history, geography, and sociology of slums and the health problems of people who live in slums. The lancet 389, 547-558, https://doi.org/10.1016/s0140-6736(16)31650-6 , 2017.

Fu, B., Wang, S., Zhang, J., Hou, Z., Li, J. Unravelling the complexity in achieving the 17 sustainable-development goals. National Science Review 6, 386-388, https://doi.org/10.1093/nsr/nwz038 , 2019.

Gram-Hansen, B.J., Helber, P., Varatharajan, I., Azam, F., Coca-Castro, A., Kopackova, V., Bilinski, P. Mapping informal settlements in developing countries using machine learning and low resolution multi-spectral data, Proceedings of the 2019 AAAI/ACM Conference on AI, Ethics, and Society, pp. 361-368, https://doi.org/10.1145/3306618.3314253 , 2019.

Guan, X., Wei, H., Lu, S., Dai, Q., Su, H. Assessment on the urbanization strategy in China: Achievements, challenges and reflections. Habitat International 71, 97-109, https://doi.org/10.1016/j.habitatint.2017.11.009 , 2018.

Guilmoto, C.Z., Rajan, S.I. Fertility at the district level in India: Lessons from the 2011 census. Economic and Political weekly, 59-70, http://www.ceped.org/wp, 2013.

Haberl H, Wiedenhofer D, Schug F, Frantz D, Virág D, Plutzar C, Gruhler K, Lederer J, Schiller G, Fishman T, Lanau M. High-resolution maps of material stocks in buildings and infrastructures in Austria and Germany. Environmental science & technology 55(5): 3368-79, https://doi.org/10.1021/acs.est.0c05642 , 2021.

Hardoy, J.E., Mitlin, D., Satterthwaite, D. Environmental problems in an urbanizing world: finding solutions in cities in Africa, Asia and Latin America. Routledge, https://doi.org/10.4324/9781315071732, 2013.

He, K., Zhang, X., Ren, S., Sun, J. Deep residual learning for image recognition, Proceedings of the IEEE conference on computer vision and pattern recognition, pp. 770-778, https://doi.org/10.1109/cvpr.2016.90 , 2016.

Hohmann, J. The right to housing: Law, concepts, possibilities. Bloomsbury Publishing, https://doi.org/10.5040/9781472566416 , 2013.

Hsu, F.-C., Baugh, K.E., Ghosh, T., Zhizhin, M., Elvidge, C.D. DMSP-OLS radiance calibrated nighttime lights time series with intercalibration. Remote Sensing 7, 1855-1876, https://doi.org/10.3390/rs70201855 , 2015.

Ibrahim, M.R., Titheridge, H., Cheng, T., Haworth, J. predictSLUMS: A new model for identifying and predicting informal settlements and slums in cities from street intersections using machine learning. Computers, Environment and Urban Systems 76, 31-56, https://doi.org/10.1016/j.compenvurbsys.2019.03.005 , 2019.

Juran, J.M., Gryna, F.M., Bingham, R.S. (1979) Quality control handbook. McGraw-Hill New York.

Li, D., Sun, L., Yu, Y., Tian, P. Geospatial micro-estimates of slum populations in 129 Global South countries using machine learning and public data. Available at https://doi.org/10.5281/zenodo.13779003, 2025.

Kingma, D.P., Ba, J. Adam: A method for stochastic optimization. arXiv preprint arXiv:1412.6980, https://doi.org/10.48550/arXiv.1412.6980, 2014.

Local Burden of Disease Educational Attainment Collaborators. Mapping disparities in education across low-and middle-income countries. Nature 577, 235-238, https://doi.org/10.1038/s41586-019-1872-1, 2020.

Mahabir, R., Agouris, P., Stefanidis, A., Croitoru, A., Crooks, A.T. Detecting and mapping slums using open data: A case study in Kenya. International Journal of Digital Earth 13, 683-707, https://doi.org/10.1080/17538947.2018.1554010 , 2020.

Marx, B., Stoker, T., Suri, T. The economics of slums in the developing world. Journal of Economic perspectives, *27*(4), 187-210, https://doi.org/10.1257/jep.27.4.187 , 2013.

Medeiros, S.d.S., Pinto, T.F., Hernan Salcedo, I., Cavalcante, A.d.M.B., Perez Marin, A.M., Tinôco, L.B.d.M. Sinopse do censo demográfico para o semiárido brasileiro. Instituto Nacional de Seminário (INSA)., http://livroaberto.ibict.br/handle/1/941, 2012.

Meena, S., Nava, L., Bhuyan, K., Puliero, S., Soares, L., Dias, H., Floris, M., Catani, F. HR-GLDD: a globally distributed dataset using generalized deep learning (DL) for rapid landslide mapping on high-resolution (HR) satellite imagery. Earth Syst. Sci. Data 15, 3283–3298, https://doi.org/10.5194/essd-15-3283-2023 , 2023.

Moreno, E.L. Slums of the world: The face of urban poverty in the new millennium?: Monitoring the millennium development goal, target 11--world-wide slum dweller estimation. Un-Habitat, https://digitallibrary.un.org/record/515731, 2003.

Mwaniki, D., Ndugwa, R. The Global Urban Monitoring Approach Taken by UN-HABITAT. Stadtentwicklung beobachten, messen und umsetzen. Informationen zur Raumentwicklung (IzR), 32-43, https://biblioscout.net/article/99.140005/izr202101003201, 2021.

Nielsen, D. Tree boosting with XGBoost: Why does XGBoost win "every" machine learning competition? Master's thesis, Norwegian University of Science and Technology, Trondheim, Norway. http://hdl.handle.net/11250/2433761,2016.

Nowak, M. Introduction to the international human rights regime. Brill, https://doi.org/10.1163/9789004479074 , 2003.

Oppenheimer, M., Campos, M., Warren, R., Birkmann, J., Luber, G., O'Neill, B., Takahashi, K., Brklacich, M., Semenov, S., Licker, R. Emergent risks and key vulnerabilities, Climate change 2014 impacts, adaptation and vulnerability: part a: global and sectoral aspects. Cambridge University Press, pp. 1039-1100, https://doi. org/10.1017/CBO9781107415379, 2015.

Owusu, M., Kuffer, M., Belgiu, M., Grippa, T., Lennert, M., Georganos, S., Vanhuysse, S. (2021) Towards user-driven earth observation-based slum mapping. Computers, environment and urban systems 89, 101681, https://doi.org/10.1016/j.compenvurbsys.2021.101681 , 2021.

Pan, S.J., Yang, Q. A survey on transfer learning. IEEE Transactions on knowledge and data engineering 22(10):1345-59, https://doi.org/10.1109/TKDE.2009.191, 2009.

Parikh, P., Parikh, H., McRobie, A. The role of infrastructure in improving human settlements. Proceedings of the Institution of Civil Engineers-Urban Design and Planning 166, 101-118, https://doi.org/10.1680/udap.10.00038 , 2013.

Patel, A., Joseph, G., Shrestha, A., Foint, Y. (2019) Measuring deprivations in the slums of Bangladesh: implications for achieving sustainable development goals. Housing and Society 46, 81-109.

Patel, N. N., Angiuli, E., Gamba, P., Gaughan, A., Lisini, G., Stevens, F. R., Tatem, A.J., Trianni, G. (2015). Multitemporal settlement and population mapping from Landsat using Google Earth Engine. International Journal of Applied Earth Observation and Geoinformation 35, 199–208. https://doi.org/10.1016/j.jag.2014.09.005.

Pedro, A.A., Queiroz, A.P. (2019) Slum: Comparing municipal and census basemaps. Habitat International 83, 30-40, https://doi.org/10.1596/32084 , 2019.

Persello, C., Kuffer, M. Towards uncovering socio-economic inequalities using VHR satellite images and deep learning, IGARSS 2020-2020 IEEE International Geoscience and Remote Sensing Symposium. IEEE, pp. 3747-3750, https://doi.org/10.1109/igarss39084.2020.9324399 , 2020.

Pesaresi, M., Ehrlich, D., Ferri, S., Florczyk, A.J., Freire, S., Halkia, M., Julea, A., Kemper, T., Soille, P., Syrris, V. Operating procedure for the production of the Global Human Settlement Layer from Landsat data of the epochs 1975, 1990, 2000, and 2014. Publications Office of the European Union Luxembourg, https://doi.org/10.2788/253582, 2016.

Ramraj, S., Uzir, N., Sunil, R., and Banerjee, S. Experimenting XGBoost algorithm for prediction and classification of different datasets. International Journal of Control Theory and Applications 9, 651–662, 2016.

Rentschler, J., Avner, P., Marconcini, M., Su, R., Strano, E., Vousdoukas, M., Hallegatte, S. Global evidence of rapid urban growth in flood zones since 1985. Nature 622, 87-92, https://doi.org/10.1038/s41586-023-06468-9 , 2023.

Robinson, C., Hohman, F., Dilkina, B. A deep learning approach for population estimation from satellite imagery, Proceedings of the 1st ACM SIGSPATIAL Workshop on Geospatial Humanities, pp. 47-54, https://doi.org/10.1145/3149858.3149863 , 2017.

Rogler, L.H. Slum Neighborhoods in Latin America. Journal of Inter-American Studies 9, 507-528, https://doi.org/10.2307/164857 , 1967.

Roy, D.P., Kovalskyy, V., Zhang, H.K., Vermote, E.F., Yan, L., Kumar, S.S. and Egorov, A. Characterization of Landsat-7 to Landsat-8 reflective wavelength and normalized difference vegetation index continuity. Remote sensing of Environment 185, 57-70, https://doi.org/10.1016/j.rse.2015.12.024 , 2016.

Russakovsky, O., Deng, J., Su, H., Krause, J., Satheesh, S., Ma, S., Huang, Z., Karpathy, A., Khosla, A., Bernstein, M. Imagenet large scale visual recognition challenge. International journal of computer vision 115, 211-252, https://doi.org/10.1007/s11263-015-0816-y , 2015.

Rutstein, S.O., Staveteig, S. Making the demographic and health surveys wealth index comparable. ICF international Rockville, MD, https://www.dhsprogram.com/pubs/pdf/MR9/MR9.pdf, 2014.

Sabry, S. Poverty lines in Greater Cairo: underestimating and misrepresenting poverty. IIED, https://www.iied.org/10572iied, 2009.

Satterthwaite, D., Archer, D., Colenbrander, S., Dodman, D., Hardoy, J., Mitlin, D., Patel, S. Building resilience to climate change in informal settlements. One Earth 2, 143-156, https://doi.org/10.1016/j.oneear.2020.02.002 , 2020.

Schetke, S., Haase, D., Kötter, T. Towards sustainable settlement growth: A new multi-criteria assessment for implementing environmental targets into strategic urban planning. Environmental Impact Assessment Review 32, 195-210, https://doi.org/10.1016/j.eiar.2011.08.008 , 2012.

Schiavina, M., Melchiorri, M., Pesaresi, M., Politis, P., Carneiro Freire, S., Maffenini, L., Florio, P., Ehrlich, D., Goch, K., Tommasi, P. GHSL data package 2022: Public release GHS P2022. KJ-07–22–357-EN-N (online), KJ-07–22–357-EN-C (print), https://doi.org/10.2760/19817, 2022.

Shi, Q., Liu, M., Marinoni, A., Liu, X. UGS-1m: Fine-grained urban green space mapping of 34 major cities in China based on the deep learning framework. Earth System Science Data Discussions 15, 555-577, https://doi.org/10.5194/essd-15-555-2023, 2023.

Sietchiping, R., Yoon, H. J. What drives slum persistence and growth? Empirical evidence from sub-Saharan Africa. International Journal of Advances Studies and Research in Africa 1, 1-22, http://www.africascience.org, 2010.

Singh, B.N. Socio-economic conditions of slums dwellers: a theoretical study. Kaav International Journal of Arts, Humanities & Social Sciences 3, 5-20, https://www.kaavpublications.org/abstract/article-236.pdf, 2016.

Smith, A., Bates, P.D., Wing, O., Sampson, C., Quinn, N., Neal, J. New estimates of flood exposure in developing countries using high-resolution population data. Nature communications 10, 1814, https://doi.org/10.1038/s41467-019-09282-y , 2019.

Stevens, F.R., Gaughan, A.E., Linard, C., Tatem, A.J. Disaggregating census data for population mapping using random forests with remotely-sensed and ancillary data. PloS one 10, e0107042, https://doi.org/10.1371/journal.pone.0107042 , 2015.

Tamiminia, H., Salehi, B., Mahdianpari, M., Quackenbush, L., Adeli, S., Brisco, B. Google Earth Engine for geo-big data applications: A meta-analysis and systematic review. ISPRS journal of photogrammetry and remote sensing 164, 152-170, https://doi.org/10.1016/j.isprsjprs.2020.04.001 , 2020.

Taubenböck, H., Wurm, M. Globale Urbanisierung–Markenzeichen des 21. Jahrhunderts. Globale Urbanisierung: Perspektive aus dem All, 5-10, https://doi.org/10.1007/978-3-662-44841-0_2 , 2015.

Tellman, B., Sullivan, J.A., Kuhn, C., Kettner, A.J., Doyle, C.S., Brakenridge, G.R., Erickson, T.A., Slayback, D.A. Satellite imaging reveals increased proportion of population exposed to floods. Nature 596, 80-86, https://doi.org/10.1038/s41586-021-03695-w , 2021.

Thomson, D.R., Kuffer, M., Boo, G., Hati, B., Grippa, T., Elsey, H., Linard, C., Mahabir, R., Kyobutungi, C., Maviti, J. Need for an integrated deprived area “slum” mapping system (IDEAMAPS) in low- and middle-income countries (LMICs). Social Sciences 9, 80, https://doi.org/10.3390/socsci9050080 , 2020.

Thomson, D.R., Linard, C., Vanhuysse, S., Steele, J.E., Shimoni, M., Siri, J., Caiaffa, W.T., Rosenberg, M., Wolff, E., Grippa, T. Extending data for urban health decision-making: a menu of new and potential neighborhood-level health determinants datasets in LMICs. Journal of urban health 96, 514-536, https://doi.org/10.1007/s11524-019-00363-3 , 2019.

Thomson, D.R., Stevens, F.R., Chen, R., Yetman, G., Sorichetta, A., Gaughan, A.E. Improving the accuracy of gridded population estimates in cities and slums to monitor SDG 11: Evidence from a simulation study in Namibia. Land Use Policy 123, 106392, https://doi.org/10.1016/j.landusepol.2022.106392, 2022.

Tian, P., Zhong, H., Chen, X., Feng, K., Sun, L., Zhang, N., Shao, X., Liu, Y. and Hubacek, K. Keeping the global consumption within the planetary boundaries. Nature, 635, 625-630, https://doi.org/10.1038/s41586-024-08154-w , 2024.

Tjia, D., Coetzee, S. Geospatial information needs for informal settlement upgrading–A review. Habitat International 122, 102531, https://doi.org/10.1016/j.habitatint.2022.102531 , 2022.

Trindade, T.C., MacLean, H.L., Posen, I.D. Slum infrastructure: Quantitative measures and scenarios for universal access to basic services in 2030. Cities 110, 103050, https://doi.org/10.1016/j.cities.2020.103050 , 2021.

UN-Habitat. The challenge of slums: global report on human settlements 2003. Management of Environmental Quality: An International Journal 15, 337-338, https://doi.org/10.1108/meq.2004.15.3.337.3 , 2004.

UN-Habitat. World Cities Report 2020: The Value of Sustainable Urbanization. https://unhabitat.org/world-cities-report-2020-the-value-of-sustainable-urbanization, 2020.

UN-habitat. Urban indicators database. https://data.unhabitat.org/pages/housing-slums-and-informal-settlements, 2021.

United Nations Conference on Trade and Development. Countries, All Groups Hierarchy, UNCTAD stat.https://unctadstat.unctad.org/EN/Classifications/DimCountries_All_Hierarchy.pdf, 2025.

~~Center for International Earth Science Information Network (CIESIN), Columbia University. Gridded Population of the World, Version 4 (GPWv4): Population Density, Revision 11. NASA SEDAC. https://doi.org/10.7927/H4F47M65, 2018.~~

Weber, H. Politics of 'leaving no one behind': contesting the 2030 Sustainable Development Goals agenda, The Politics of Destination in the 2030 Sustainable Development Goals. Routledge, pp. 64-79, https://doi.org/10.4324/9780429490507-4 , 2018.

Wisner, B. Vulnerability as concept, model, metric, and tool, Oxford research encyclopedia of natural hazard science, https://doi.org/10.1093/acrefore/9780199389407.013.25, 2016.

World Bank. World Bank country and lending groups https://datahelpdesk.worldbank.org/knowledgebase/articles/906519, 2022.

World Bank Group. Population living in slums (% of urban population). https://data.worldbank.org/indicator/EN.POP.SLUM.UR.ZS, 2018.

Wu, Z., Shen, C., Van Den Hengel, A. Wider or deeper: Revisiting the resnet model for visual recognition. Pattern recognition 90, 119-133, https://doi.org/10.1016/j.patcog.2019.01.006 , 2019.

Wulder, M. A., Roy, D. P., Radeloff, V. C., Loveland, T. R., Anderson, M. C., Johnson, D. M., Healey, S., Zhu, Z., Scambos, T. A., Pahlevan, N., Hansen, M., Gorelick, N., Crawford, C. J., Masek, J. G., Hermosilla, T., White, J. C., Belward, A. S., Schaaf, C., Woodcock, C. E., Huntington, J. L., Lymburner, L., Hostert, P., Gao, F., Lyapustin, A., Pekel, J.-F., Strobl, P., Cook, B. D. (2022). Fifty years of Landsat science and impacts. Remote Sensing of Environment 280, 113195. https://doi.org/10.1016/j.rse.2022.113195~~Wulder, M.A., Roy, D.P., Radeloff, V.C., Loveland, T.R., Anderson, M.C., Johnson, D.M., Healey, S., Zhu, Z., Scambos, T.A., Pahlevan, N. Fifty years of~~

~~Landsat science and impacts. Remote Sensing of Environment 280, 113195, https://doi.org/10.1016/j.rse.2022.113195 , 2022~~.

Wurm, M., Stark, T., Zhu, X.X., Weigand, M., Taubenböck, H. Semantic segmentation of slums in satellite images using transfer learning on fully convolutional neural networks. ISPRS journal of photogrammetry and remote sensing 150, 59-69, https://doi.org/10.1016/j.isprsjprs.2019.02.006 , 2019.

Wurm, M., Taubenböck, H., Weigand, M., Schmitt, A. Slum mapping in polarimetric SAR data using spatial features. Remote sensing of environment 194, 190-204, https://doi.org/10.1016/j.rse.2017.03.030 , 2017.

Yeh, C., Perez, A., Driscoll, A., Azzari, G., Tang, Z., Lobell, D., Ermon, S., Burke, M. Using publicly available satellite imagery and deep learning to understand economic well-being in Africa. Nature communications 11, 2583, https://doi.org/10.1038/s41467-020-16185-w , 2020.

Zhou, Y., Li, X., Chen, W., Meng, L., Wu, Q., Gong, P., Seto, K.C. Satellite mapping of urban built-up heights reveals extreme infrastructure gaps and inequalities in the Global South. Proceedings of the National Academy of Sciences 119, e2214813119, https://doi.org/10.1073/pnas.2214813119 , 2022.